

Synthesis of Magnesium Oxide Nanomaterial and Employing it as an Electrochemical Probe for Hydroxyl Radical



CHE
2047

A Dissertation Submitted to the Department of Chemistry, Quaid-i-Azam University,
Islamabad, for the Partial Fulfillment of the Requirements for the Degree

of

Master of Philosophy

In

Physical Chemistry

By

ABDUL KARIM

**Department of Chemistry
Quaid-i-Azam University
Islamabad 45320, Pakistan.**

2022

DECLARATION

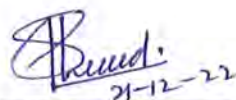
This is to certify that this dissertation entitled “**Synthesis of Magnesium Oxide Nanomaterial and Employing it as an Electrochemical Probe for Hydroxyl Radical**” submitted by *Mr. Abdul Karim*, is accepted in its present form by the Department of Chemistry, Quaid-i-Azam University, Islamabad, as satisfying the dissertation requirements for the degree of *Master of Philosophy in Physical Chemistry*.

External Examiner:



Dr. Azra Yaqub
Senior Scientist
Chemistry Division
Directorate of Science, PINSTECH.
P.O. Nilore, Islamabad.

Supervisor:



Prof. Dr. Safer Ahmed
Department of Chemistry
Quaid-i-Azam University
Islamabad

Head of Section:



Prof. Dr. Hazrat Hussain
Department of Chemistry
Quaid-i-Azam University
Islamabad

Chairman:



Prof. Dr. Aamer Saeed Bhatti
Department of Chemistry
Quaid-i-Azam University
Islamabad

بِسْمِ اللَّهِ الرَّحْمَنِ الرَّحِيمِ

Al-Quran

Say (O Muhammad ﷺ): "Tell me! If (all) your water was to be sunk away, who then can supply you with flowing (spring) water?"

67:30

DEDICATION

I dedicate this effort to my parents,
Mr. and Mrs. Feroz Uddin Kazi,
my supervisor **Prof. Dr. Safeer Ahmed,**
my teachers and friends.

Thanks for your endless support,
trust, and prayers.

Acknowledgments

All praises to **Allah Almighty**, the most Beneficent and Merciful, who bestowed His blessings and the mediation of His Beloved **Prophet Hazrat Muhammad (P.B.U.H)** enlightened me with great resoluteness and perseverance, that enabled me to accomplish this scientific assignment objectively and successfully. His blessings always enabled me to stand in my life with determination and success.

I feel great pleasure in expressing my profound gratitude to my supervisor **Prof. Dr. Safeer Ahmed**, Department of Chemistry, Quaid-i-Azam University, Islamabad, for his constructive counseling, valuable suggestions, and faith in my mere approaches to work. He streamlined my efforts towards research work. I would also like to express my sincere appreciation to **Prof. Dr. Aamer Saeed Bhatti** (Chairman of the Department of Chemistry) and **Prof. Dr. Hazrat Hussain** (Head of the Physical Section) for providing me with lab facilities.

Apart from these personalities, I would like to acknowledge sincere indebtedness and gratitude to all **my respected teachers** for their moral support and for making me what I am today. I am also very grateful to my **lab fellows and friends** for their support and encouragement throughout my research. No deeds can return, and no word can express the affection, love, amiable sacrifices, unceasing prayers, advice, inspiration, and support my **Family** infused in me throughout my academic career and life. I am grateful to my father and mother for their endless love, guidance, and valuable suggestions during the entire coursework. Finally, I would say thanks to all who have been supportive and cooperative. May **Allah** bless you all; **Allah** is the only one who promises “the reward for good [anything] but good.”

Abdul Karim

Table of contents

List of figures.....	ix
List of tables.....	xi
List of abbreviations	xii
ABSTRACT.....	xiv
CHAPTER 01	1
INTRODUCTION.....	1
1.1 Free radicals	1
1.1.1 Classification of free radicals	2
1.1.1.1 Reactive oxygen species (ROS).....	2
1.1.1.2 Reactive nitrogen species (RNS)	4
1.1.2 Sources of free radicals.....	4
1.1.2.1 Exogenous sources.....	5
1.1.2.2 Endogenous sources.....	5
1.1.3 Oxidative stress and pathological role of free radicals.....	6
1.1.3.1 Diabetes mellitus.....	7
1.1.3.2 Neurodegenerative diseases	7
1.1.3.3 Cancer	7
1.2 Fenton chemistry	8
1.3 Detection of free radicals	9
1.3.1 Direct detection.....	11
1.3.2 Indirect detection	11
1.4 Sensors	11
1.4.1 Biosensors.....	12
1.4.2 Physical sensors.....	12
1.4.3 Chemical sensors	12
1.4.3.1 Optical sensors.....	13

1.4.3.2 Thermometric sensors	13
1.4.3.3 Mass-sensitive sensors	13
1.4.3.4 Electrochemical sensors	14
1.5 Protein immobilized polymer-modified electrodes	14
1.5.1 Physisorption	15
1.5.2 Chemisorption	15
1.5.3 Film deposition	15
1.6 Magnesium oxide (MgO)	15
1.7 Literature review	17
1.8 Aim of work	20
CHAPTER 02	21
EXPERIMENTAL	21
2.1 Chemicals and reagents	21
2.2 Instrumentation	22
2.2.1 Electrochemical workstation	22
2.2.2 UV-Visible spectrometer	23
2.2.3 X-ray diffraction (XRD) analysis	23
2.2.4 Scanning electron microscope coupled with Energy dispersive x-ray spectroscopy (SEM+EDX)	24
2.3 Experimental procedure	24
2.3.1 Synthesis of MgO nanomaterials	24
2.3.2 Fabrication of the electrodes	25
2.3.2.1 Activation of graphite	25
2.3.2.2 Fabrication of carbon paste electrodes (CPEs)	26
2.3.2.3 Physical cleaning of the electrodes	27
2.3.3 Surface modification of the fabricated electrodes	27
2.3.3.1 Electropolymerization of o-phenylenediamine	27

2.3.3.2 Immobilization of Bovine serum albumin (BSA).....	29
2.4 Electrochemical detection of hydroxyl radical on the designed sensing platform.....	30
CHAPTER 03	32
RESULTS AND DISCUSSION	32
3.1 Characterization of the synthesized nanomaterials	32
3.1.1 X-ray diffraction analysis	32
3.1.2 Scanning electron microscopy and Energy dispersive X-ray spectroscopy	34
3.2 UV-Visible spectroscopic analysis.....	35
3.3 Electropolymerization of o-phenylenediamine (o-PD)	37
3.4 Electrochemical examination of the fabricated electrochemical probes	40
3.4.1 Electrochemical characterization using cyclic voltammetry	40
3.4.2 Electrochemical characterization using electrochemical impedance spectroscopy	43
3.5 Electrochemical examination of PoPD-modified electrodes	44
3.5.1 Cyclic voltammetric examination.....	44
3.5.2 Square wave voltammetric examination.....	45
3.6 Square wave voltammetric investigation of PoPD-modified electrodes.....	46
3.7 Electrochemical probing of hydroxyl free radical.....	47
3.7.1 Square wave voltammetric investigation.....	47
3.7.1.1 Oxidative damage by hydroxyl radical	49
3.7.1.2 Oxidative damage of BSA in H ₂ O ₂ , Fe ²⁺ , or the Fenton system	50
3.7.2 Electrochemical impedance spectroscopic investigation	52
CONCLUSION	54
REFERENCES.....	55

List of figures

Figure 1.1 Classification of biological by-products.....	2
Figure 1.2 Exogenic contributors of the free radicals. ⁵	5
Figure 1.3 Endogenous sources of the free radicals. ⁵	6
Figure 1.4 Methods for detection of free radicals.....	10
Figure 1.5 Phenomena exhibited by MgO at the nanoscale. ¹¹⁷	17
Figure 2.1 Electrochemical workstation connected with a voltammetric cell.	22
Figure 2.2 Pictorial representation of the synthesis of MgO nanomaterials.....	25
Figure 2.3 Pictorial illustration of the electrode fabrication process.	26
Figure 2.4 The fabricated carbon paste electrodes (CPEs).	27
Figure 2.5 Cyclic voltammograms of six consecutive scans obtained for electropolymerization.	28
Figure 2.6 Pictorial illustration of the electropolymerization of o-PD.	29
Figure 2.7 Pictorial illustration of the process of immobilizing BSA on PoPD-modified electrodes.	29
Figure 2.8 BSA immobilization on PoPD-modified electrodes.....	30
Figure 2.9 Pictorial illustration of the Hydroxyl attack on the BSA immobilized PoPD- modified electrodes.....	30
Figure 2.10 Hydroxyl free radical attack on BSA immobilized PoPD modified electrodes. .	31
Figure 3.1 XRD patterns of synthesized undoped MgO and Zn ²⁺ doped MgO along with standard pattern obtained from JCPDS card no. 78-0430.....	32
Figure 3.2 (A, B) SEM micrographs and (C) EDX spectrum of synthesized MgO nanomaterial.	34
Figure 3.3 UV-Vis spectrum of (A) methyl violet (MV), (B) MV + Fe ²⁺ , (C) MV + H ₂ O ₂ , and (D) MV + H ₂ O ₂ + Fe ²⁺ , with concentration MV 0.06 mM, Fe ²⁺ 12 mM, and H ₂ O ₂ 45 mM respectively.	35
Figure 3.4 Cyclic voltammograms of electropolymerization of 0.5 mM o-PD in 0.50 M sulfuric acid on (A) GCE, (B) CPE, (C) MgO/CPE, (D) Mg _{0.98} Zn _{0.02} O/CPE, (E) Mg _{0.96} Zn _{0.04} O/CPE, (F) Mg _{0.94} Zn _{0.06} O/CPE, (G) Mg _{0.92} Zn _{0.08} O/CPE, and (H) Mg _{0.90} Zn _{0.10} O/CPE.....	38

Figure 3.5 Cyclic voltammograms of (A) CPE and (B) MgO/CPE, obtained in 5mM of $K_3[Fe(CN)_6]$ (redox probe) in 0.1M KCl (supporting electrolyte) at a scan rate of 100 mV/s.	40
Figure 3.6 (A) Cyclic voltammograms of CPE obtained at different scan rates, (B) a plot of I_p vs. $v^{1/2}$ of CPE, (C) cyclic voltammograms of MgO/CPE obtained at different scan rates, and (D) a plot of I_p vs. $v^{1/2}$ of MgO/CPE.	42
Figure 3.7 (A) Nyquist plot of CPE and MgO/CPE in a solution of 5 mM $K_3[Fe(CN)_6]$ in 0.1M KCl, and (B) Equivalent EIS circuit.	43
Figure 3.8 Cyclic voltammogram of PoPD-modified electrode at a scan rate of 100 mV/s. .	45
Figure 3.9 Square wave voltammogram of PoPD-modified electrode.	45
Figure 3.10 (A) Square wave voltammetric responses of polymer-modified electrodes, and (B) bar graph representing peak current responses of different electrodes.	46
Figure 3.11 Square wave voltammograms of fabricated electrodes (A) PoPD-modified MgO/CPE, (B) BSA immobilized PoPD-modified MgO/CPE, and (C) BSA immobilized-PoPD modified MgO/CPE after hydroxyl attack.	48
Figure 3.12 Square wave voltammograms of PoPD/MgO/CPE and BSA@PoPD/MgO/CPE in the absence and presence of hydroxyl free radical.	49
Figure 3.13 Square wave voltammograms of BSA@PoPD/MgO/CPE in the absence and presence of Fe^{2+} , H_2O_2 , or Fenton system.	51
Figure 3.14 (A) Nyquist plot of BSA immobilized PoPD-modified MgO electrode and (B) Equivalent EIS circuit.	52

List of tables

Table 1.1 ROS and RNS produced during metabolic processes. ⁶⁶	10
Table 1.2 Properties of MgO (bulk). ¹⁰⁵	16
Table 2.1 The chemicals/reagents and their specifications.	21
Table 3.1 Average crystallite sizes of synthesized nanomaterials.	34
Table 3.2 Comparison of the oxidation peak current of electropolymerization of o-phenylenediamine using cyclic voltammetry on different electrodes.....	39
Table 3.3 Cyclic voltammetric data of CPE and MgO/CPE.	42
Table 3.4 Parameters obtained from EIS.	44
Table 3.5 Square wave voltammetric response of PoPD-modified electrodes.	47
Table 3.6 Square wave voltammetric response of protein immobilized polymer modified electrode.	49
Table 3.7 Square wave voltammetric response of polymer and protein modified electrodes pre and post hydroxyl attack.	50
Table 3.8 Square wave voltammetric data of BSA@PoPD/MgO/CPE.....	51
Table 3.9 Parameters obtained from EIS.	53

List of abbreviations

AGEs	Advanced glycation end products
AC	Alternating current
ATP	Adenosine triphosphate
BSA	Bovine serum albumin
BSA@PoPD/MgO/CPE	Bovine serum albumin immobilized poly-o-phenylenediamine modified carbon paste electrode
CNS	Central nervous system
CPE	Carbon paste electrode
CV	Cyclic voltammetry
DNA	Deoxyribonucleic acid
1,3-DPG	1,3-Diphosphoglycerate
DET	Direct electron transfer
ED	Electrochemical detection
EDX	Energy dispersive x-ray
EIS	Electrochemical impedance spectroscopy
EPR	Electron paramagnetic resonance
FWHM	Full width at half maximum
GSH	Glutathione
GP	Glutathione peroxidase
GR	Glutathione reductase
G3P	Glycerol-3-phosphate
H. W. reaction	Haber Weis reaction
HOMO	Highest occupied molecular orbital
HPLC	High-pressure liquid chromatography
8-OhdG	8-Hydroxyguanosine
ICDD	International centre for diffraction data
JCPDS	Joint committee on powder diffraction standards
LUMO	Lowest unoccupied molecular orbital
MgO/CPE	Magnesium oxide-based carbon paste electrode

MV	Methyl violet
NADH	Nicotinamide adenine dinucleotide
NOS	Nitric oxide synthase
o-PD	o-Phenylene diamine
PBS	Phosphate buffer saline
PANI	Polyaniline
PIN	Polyindole
PoPD	Poly-o-phenylene diamine
Ppy	Polypyrrole
PT	Polythiophene
PVC	Polyvinyl chloride
RNS	Reactive nitrogen species
ROS	Reactive oxygen species
SCE	Saturated calomel electrode
SEM	Scanning electron microscopy
SHE	Standard hydrogen electrode
SOD	Superoxide dismutase
SWV	Square wave voltammetry
UV-Vis	Ultraviolet-visible
XRD	X-ray diffraction
ZnMgO/CPE	Zinc-doped magnesium oxide-based carbon paste electrode

ABSTRACT

A protein-modified carbon paste electrode (CPE) consisting of two separate layers of inorganic magnesium oxide (MgO) nanomaterial and organic poly-*o*-phenylenediamine (PoPD) was designed for the electrochemical detection of short-lived hydroxyl radical ($\cdot\text{OH}$). The hydroxyl radical is a type of reactive oxygen species (ROS). The generation of hydroxyl radical in the living system was mimicked using the Fenton reaction and was confirmed using UV-Visible spectroscopy. The high reactivity of the hydroxyl radical enables it to impart oxidative damage to the bovine serum albumin (BSA) immobilized on the surface of the fabricated electrochemical sensing platform. The monitoring of the oxidative damage served as an indirect measure of the presence of hydroxyl radicals in the medium. The signals generated from the interaction of the hydroxyl radical with the recognition layer of the proposed electrochemical sensing scaffold were characterized using square wave voltammetry (SWV) and electrochemical impedance spectroscopy (EIS). Undoped and Zn^{2+} doped MgO nanomaterials were synthesized using the fuel combustion method and were used for fabricating carbon paste electrodes. Cyclic voltammetry (CV) was employed to execute the electropolymerization of *o*-phenylenediamine (*o*-PD) on the MgO-based CPE to promote facile electron transfer between the anchored protein and the electrode's surface. The degradation of the immobilized protein was investigated in the presence of the solution of hydrogen peroxide, ferrous (Fe^{2+}) salt, and a combination of both to elucidate the efficiency of the proposed sensing platform. Although the proposed electrochemical probing platform demonstrated high selectivity for the hydroxyl radical, it can only be used once owing to the loss of native characteristics of the immobilized protein post hydroxyl free radical attack. The fabricated BSA immobilized PoPD-modified MgO-based CPE (BSA@PoPD/MgO/CPE) sensing platform possesses the ability to detect the abnormal overexpression of the hydroxyl radicals in a living system to prevent pathological disorders encountered at later stages of life.

CHAPTER 01

INTRODUCTION

The population of the world is increasing expeditiously. The ever-growing number of living beings in the biosphere will ultimately lead to a scarcity of necessities such as food, water, shelter, etc. Different small and large-scale industries have been set up to address the issues of the escalating population. On the one hand, these industries promote ease of living by producing a wide variety of products. But on the other hand, they serve as major contributors to environmental pollution. In recent years, anthropogenic environmental pollution and its effects on health have become a serious concern to the scientific community all over the globe.¹ The exogenous sources, such as the discharge of toxic gases and untreated industrial effluents, result in the adulteration of air and water bodies, posing a serious risk to aquatic and terrestrial organisms.² Life is built on a chemical foundation;³ this suggests that every living system is composed of atoms that undergo chemical reactions to maintain normal metabolism and produce energy in the cells. Flora and fauna exposed to a contaminated environment are at greater risk of developing different biological abnormalities capable of disrupting the normal functioning of the biological system.⁴ The endogenous sources include the endoplasmic reticulum, mitochondria, and peroxisomes, owing to the metabolic reactions taking place in them along with the exogenous sources, result in the production of a number of oxygen-based reactive species which at higher concentrations are capable of damaging macromolecules by inducing DNA damage, protein modification, and lipid peroxidation.⁵ The biomonitoring of the abnormal overexpression of the reactive oxygen species (ROS) at early stages can serve as a biomarker for preventing the complexities such as Atherosclerosis,⁶ Cancer,⁷ Parkinson's disease,⁸ Alzheimer's disease,⁹ etc., appearing at later stages of life.

1.1 Free radicals

Free radicals are chemical species, i.e., atoms or molecules consisting of an unpaired electron in their valence atomic or molecular orbital.¹⁰ The homolytic cleavage of covalent bonds results in the generation of free radicals. A free radical is capable of existing independently. The availability of an unpaired electron in their electron cloud imparts them with high reactivity, low stability, and a short lifetime.¹¹ These highly reactive chemical moieties acquire stability either by donating or abstracting electrons from other molecules, therefore can act as an oxidant or a reductant. They are generated as a result of normal metabolic reactions. Free radicals exhibit a dual role as both beneficial and lethal species in

living organisms. Free radicals are valuable at low or moderate concentrations because they protect against microorganisms, aid mitogenic responses, and facilitate redox regulation in the living system.¹² But at higher concentrations, they result in oxidative stress and serve as a potential threat to biomolecules. The primary and secondary free radicals react with macromolecules, such as proteins, lipids, nucleic acids, etc., which are readily available in the biological system.¹³ A free radical's reaction with a non-radical chemical moiety initiates a chain reaction, wherein the non-radical chemical specie ends up being transformed into a free radical. The reaction and linking of the two free radicals by forming a covalent bond mark the end (termination) of the reaction.¹⁴

1.1.1 Classification of free radicals

The free radicals generated during the metabolic processes have been categorized into reactive oxygen species (ROS) and reactive nitrogen species (RNS). The hierarchical diagram shown in **Figure 1.1** represents the classification of the by-products generated in a living system.

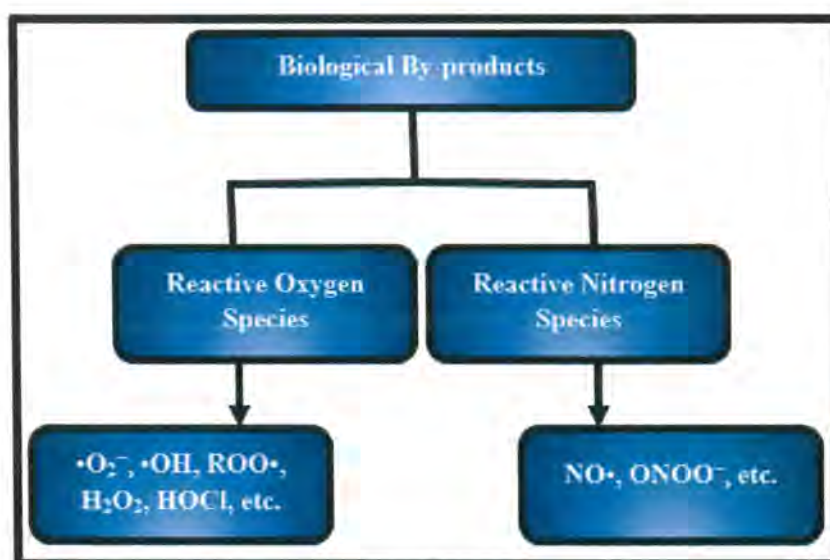


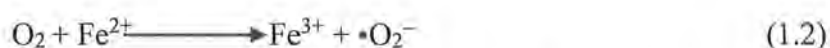
Figure 1.1 Classification of biological by-products.

1.1.1.1 Reactive oxygen species (ROS)

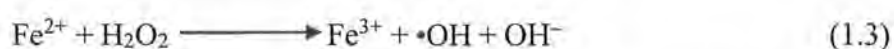
It is a class of free radicals and other chemically reactive moieties derived from oxygen during different metabolic processes. Oxygen is an element of importance for aerobic living organisms because it facilitates the generation of Adenosine triphosphate (ATP) in the mitochondrial electron transport chain in living cells and regulates different metabolic

processes.⁵ This class includes the superoxide anion radical ($\bullet\text{O}_2^-$), hydroxyl radical ($\bullet\text{OH}$), perhydroxyl radical ($\text{HOO}\bullet$), hydrogen peroxide (H_2O_2), etc.

In biological systems, the superoxide anion radical ($\bullet\text{O}_2^-$) is the most abundant free radical, which is generated during enzymatic (autooxidation) and non-enzymatic reactions by transferring an electron to an oxygen molecule.¹⁵ It is produced in mitochondria and is comparatively less reactive than other reactive oxygen species. The enzymes that promote the generation of $\bullet\text{O}_2^-$ include xanthine oxidase,¹⁶ lipoxygenase,¹⁷ cyclooxygenase,¹⁸ and nicotinamide-adenine dinucleotide phosphate (NADPH) dependent oxidase.¹⁹ Under physiological conditions, it acts as a reducing or oxidizing agent. As a reductant, the superoxide anion radical reduces iron (Fe) based complexes such as cytochrome-c and ferric-ethylene diaminetetraacetic acid (Fe^{+3} -EDTA). It possesses the capability to oxidize ascorbic acid and tocopherol. The generation of superoxide anion radical follows the reactions shown in **Equation 1.1 and 1.2**.



The hydroxyl radical ($\bullet\text{OH}$) is a highly reactive free radical and neutral form of hydroxyl ion (OH^-).²⁰ In comparison to other ROS, hydroxyl free radical causes severe damage to the living system owing to its ability to react with essential biological molecules, such as DNA, carbohydrates, lipids, proteins, etc.²¹ It is generated by the Fenton reaction,²² wherein hydrogen peroxide reacts with transition metal ions, such as cuprous (Cu^+) or ferrous (Fe^{2+}) ions, which are mostly bound to different proteins such as ferritin and ceruloplasmin. The excess of superoxide anion radical in the biological system causes the release of Fe^{2+} ions from ferritin, and the released metal ions react with H_2O_2 to produce $\bullet\text{OH}$ radicals.²³ The hydroxyl free radicals are formed by the Fenton reaction shown in **Equation 1.3**.



The perhydroxyl radical ($\text{HOO}\bullet$) is the simplest form of peroxy radical ($\text{ROO}\bullet$). The protonation of the superoxide anion radicals yields perhydroxyl radicals.²⁴ It is responsible for initiating the peroxidation of the fatty acid and promotes tumor development.²⁵

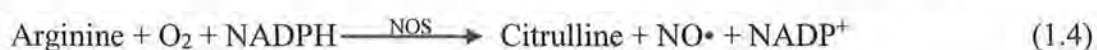
Hydrogen peroxide (H_2O_2) is not a free radical. In a living system, the superoxide dismutase enzyme catalyzes a dismutation reaction during which hydrogen peroxide is

produced.²⁶ It is hazardous at concentrations as low as 10 μM . At higher concentrations, H_2O_2 causes inactivation and denaturing of energy-producing enzymes such as glyceraldehyde-3-phosphate. Hydrogen peroxide possesses the ability to penetrate the membranes of the cells. The major antioxidants capable of eliminating H_2O_2 are catalase,²⁷ glutathione peroxidase,²⁸ and peroxiredoxins.²⁹

1.1.1.2 Reactive nitrogen species (RNS)

It is a class of free radicals and other chemical species derived from nitrogen during different metabolic processes. This class includes nitric oxide radical ($\text{NO}\cdot$), peroxynitrite ion (ONOO^-), nitrosonium cation (NO_2^{++}), etc.³⁰

In a biological system, a class of enzymes known as nitric oxide synthase (NOS) facilitates the generation of nitric oxide or nitrogen monoxide radicals during the transformation of arginine to citrulline.³¹ The $\text{NO}\cdot$ radical is generated due to oxidation of terminal guanidino nitrogen atoms. Neuronal, endothelial, and inducible NOS, facilitate the formation of $\text{NO}\cdot$ radical. It possesses the ability to diffuse through the cytoplasm and plasma membrane owing to its solubility in aqueous and lipid-based media.³² Nitric oxide radical facilitates guanylate cyclase, protein kinases, and the relaxation of muscles. It acts as a redox regulator,³³ and regulates the activity of the enzymes by regulating nitrosylation of proteins.³⁴ The production of $\text{NO}\cdot$ in a living system follows the reaction given in **Equation 1.4**.



The reaction of the superoxide anion radical with nitrogen monoxide radical yields peroxynitrite radical. It possesses high toxicity and reacts with carbon dioxide (CO_2) to form highly reactive nitroso peroxocarbonate (ONOOCO_2^-) or peroxynitrous acid (ONOOH). The $\cdot\text{OH}$ radical and NO_2 are produced as a result of dissociation of peroxynitrous acid or, on rearrangement, yields NO_3ONOO^- that oxidizes lipids, methionine, and tyrosine in proteins and oxidizes DNA to nitroguanine.³⁵

1.1.2 Sources of free radicals

The exogenous and endogenous sources contribute to the generation of these highly reactive chemical species. The sources of free radicals have been discussed in the subsequent sections.

1.1.2.1 Exogenous sources

Living organisms are exposed to ever-worsening environmental conditions, which serve as exogenous sources for producing free radicals in the biological system. The exogenous sources include consumption and inhalation of pesticides, herbicides, contaminated air and water, drinking alcohol, smoking cigarettes, exposure to ultraviolet and gamma radiations, and use of chemotherapeutic drugs (e.g., doxorubicin, cyclosporine).³⁶ The external factors contributing to the generation of free radicals have been mentioned in **Figure 1.2**.

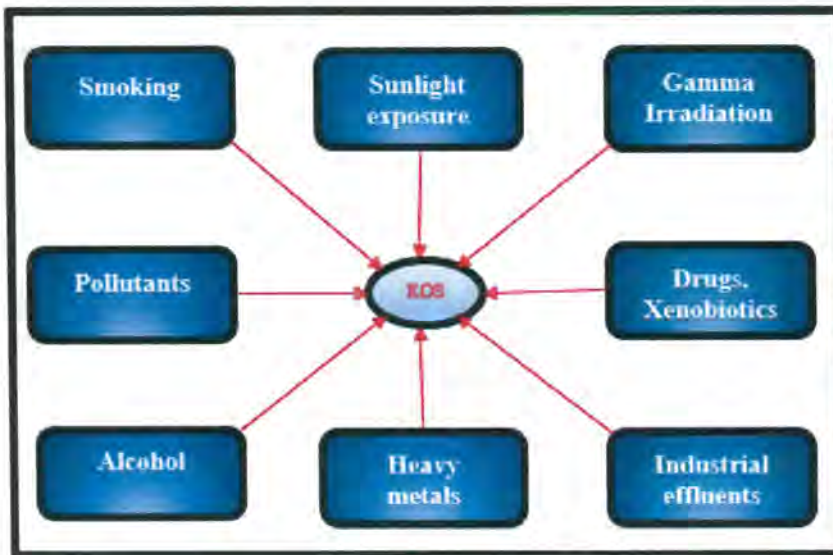


Figure 1.2 Exogenic contributors of the free radicals.⁵

1.1.2.2 Endogenous sources

The enzymatic and non-enzymatic metabolic reactions that occur in a living system result in the production of free radicals. The endogenous sources include cell organelles such as mitochondria, endoplasmic reticulum, peroxisomes, etc., wherein oxygen consumption is high.

The metabolic processes in mitochondria are the major contributors to the free radicals in a living organism. During energy generation in the electron transport chain, about 1-3% of electrons interact with molecular oxygen prematurely to form superoxide anion radicals.³⁷ The generation of superoxide anion radicals in the mitochondria damages the mitochondrial protein, lipids, and DNA. The damaged lipids of the mitochondria transform into cross-linked compounds, which are stored in the form of fine yellow-brown pigment granules known as lipofuscin.³⁸

The endoplasmic reticulum consists of a class of enzymes called cytochrome P450 mixed-function oxidase.³⁹ These enzymes can oxidize various chemical species found in the biological system. Before oxidation, the oxidase enzymes reduce oxygen to the superoxide anion radical. Some superoxide anion radicals diffuse away from the enzymes before enforcing oxidation in the reaction.⁴⁰

The peroxisomes are the membrane-enclosed organelles of a living cell. These are rich in different enzymes capable of oxidizing many substrates in the living system. Various biological molecules, such as amino acids, fatty acids, and uric acid, are metabolized here, producing hydrogen peroxide.⁴¹ The large amount of hydrogen peroxide produced in peroxisomes is scavenged by the catalase enzyme. The major endogenous contributors to the free radical generation have been shown in **Figure 1.3**.

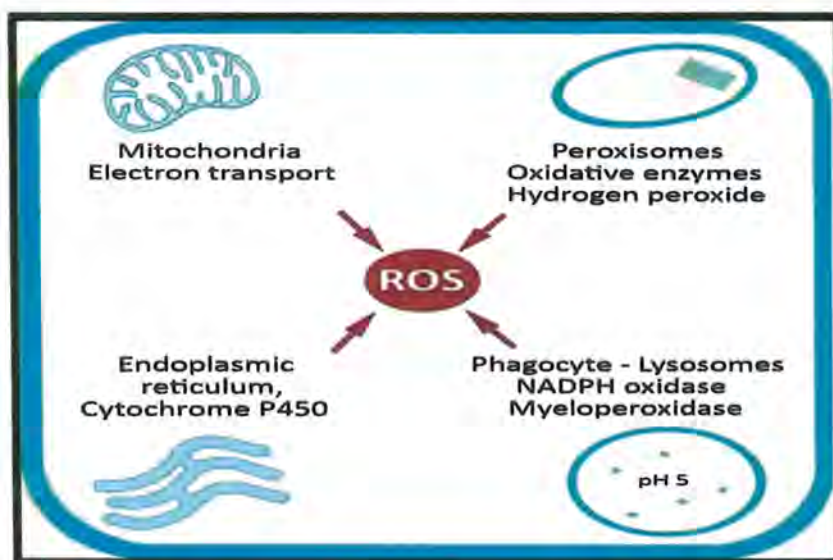


Figure 1.3 Endogenous sources of the free radicals.⁵

1.1.3 Oxidative stress and pathological role of free radicals

The effects of the overexpression or overgeneration of free radicals during metabolic processes are eradicated by antioxidant defense systems. The enzymes, such as superoxide dismutase (SOD),⁴² glutathione reductase (GR),⁴³ glutathione peroxidase (GP),⁴⁴ catalase,⁴⁵ etc., serve as endogenous antioxidants, whereas the exogenous antioxidants include Vitamin A, C, and E.⁴⁶ The complete elimination of ROS and RNS by the cells is impossible because they are beneficial up to a certain tolerance limit. Oxidative stress is a biological condition that corresponds to the imbalance of oxidants and antioxidants arising due to either an increase in the free radical concentration, decreased concentration of the available antioxidants, or both.⁴⁷

The components of the biological systems under oxidative stress cannot nullify the toxicity of the reactive intermediates and repair the triggered damage. The living system under oxidative stress is prone to encounter pathological disorders.⁴⁸

1.1.3.1 Diabetes mellitus

It is a chronic disorder; the symptoms include elevated blood glucose levels (hyperglycemia) due to insufficient insulin expression by beta cells of the pancreas (Type I diabetes), confrontation to insulin activity (Type II diabetes), or both.⁴⁹ The hyperglycemic condition promotes the free radical generation following four (04) pathways,⁵⁰ namely, 1) enhanced glycolysis (conversion of glucose to pyruvate), which results in the oxidation of glycerol-3-phosphate (G3P) to 1,3-diphosphoglycerate (1,3-DPG) and pronounced NADH/NAD⁺ ratio, 2) Polyol pathway, which facilitates the accretion of sorbitol and fructose resulting in a decrease in the glutathione (GSH) concentration and augmented NADH/NAD⁺ ratio, 3) auto-oxidation of glucose, which results in the generation of different chemical moieties such as hydroxyl radical, superoxide anion radical and ketoaldehydes, 4) protein glycation (non-enzymatic), which facilitates the formation of advanced glycation end products (AGEs) capable of interacting with the receptors and result in oxidative stress.

1.1.3.2 Neurodegenerative diseases

The cerebrospinal nervous system (CNS) is a vital component of living organisms. It is most susceptible to oxidant attack because it is rich in lipids, involves rapid oxygen utilization, and has low levels of antioxidant enzymes.⁵¹ The peroxidation of lipids by ROS increases the membrane's permeability for ions and decreases the membrane's potential and fluidity. The regions of the brain, such as the hippocampus, substantia nigra, and striatum, are prone to free radical's attacks. Oxidative stress promotes neurodegenerative diseases, such as Alzheimer's disease,⁵² Parkinson's disease,⁵³ Sclerosis,⁵⁴ etc.

1.1.3.3 Cancer

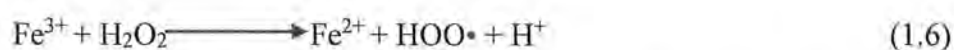
Free radicals can initiate different chemical changes in the DNA by promoting alterations in its nitrogenous bases, deletions, and chromosomal rearrangements; thus, they are mutagenic and promote cancer.⁵⁵ In comparison to the normal cells, the cancerous cells are rich in ROS and prone to mitochondrial dysfunction owing to their high metabolic rate. The activation of the oncogenes and a decreased expression of tumor suppressors result in the generation of oxidative stress in the cancer-affected cells. Reactive oxygen species alter the growth signals and gene expression resulting in the propagation of cancerous cells.⁵⁶

1.2 Fenton chemistry

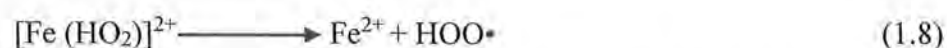
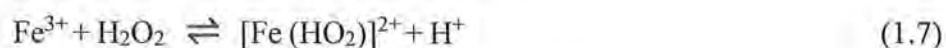
It was reported by H.J.H Fenton that the oxidation of malic acid (MA) by hydrogen peroxide is strongly promoted by ferrous (Fe^{2+}) ions.⁵⁷ The combined effect of H_2O_2 and Fe^{2+} is known as the Fenton reaction. Later it was suggested by Haber and Weiss that the hydroxyl radical was the actual oxidant in such systems.⁵⁸ Therefore, the Fenton reaction is also known as the Haber-Weiss reaction (H. W. reaction). In the mid-1960s, Merz, Waters, and Walling reported stoichiometric relations about the H. W. reaction, which were used to determine the relative susceptibilities of different organic compounds to the hydroxyl radical's attack.

Transition metal ions, such as those of iron (Fe^{2+}), on reaction with hydrogen peroxide, result in the generation of hydroxyl radical.⁵⁹ Hydroxyl radical is the strongest oxidizing agent in the biological system and the second strongest oxidizing agent after fluorine ($E^\circ=2.8$ V vs. SHE).⁶⁰ The hydroxyl radical's production by following the Fenton reaction is shown in **Equation 1.3 (Section 1.1.1.1)** of this chapter.

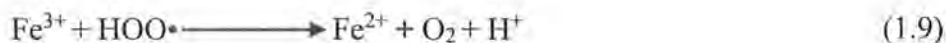
The ferric (Fe^{3+}) ion generated in the Fenton reaction can be converted into a ferrous (Fe^{2+}) ion by following different pathways in biological systems.⁶⁰ The superoxide anion radical produced as a result of metabolic activities can react with Fe^{3+} ion to reduce it to Fe^{2+} ion following the reaction shown in **Equation 1.5**, the produced Fe^{3+} ion also possesses the ability to react with H_2O_2 and is converted to Fe^{2+} ion following a Fenton-like reaction shown in **Equation 1.6**, or the Fe^{3+} ions react with the perhydroxyl radicals which result in the reduction of former to Fe^{2+} as suggested in **Equation 1.9**.



Equation 1.6 involves a two-step transformation, wherein $[\text{Fe}(\text{HO}_2)]^{2+}$ is formed at the equilibrium, then converted to Fe^{2+} and $\text{HOO}\bullet$. The mechanism of the reaction is given in **Equations 1.7 and 1.8**.



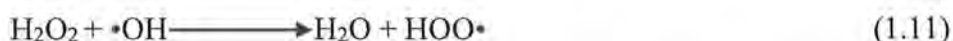
The $\text{HOO}\bullet$ formed in the Fenton-like reaction is not highly reactive and does not pose a greater threat to the biological macromolecules at lower concentrations as compared to $\bullet\text{OH}$.



The biologically important chemical species found in the living systems are prone to hydroxyl radical's attack, resulting in the generation of dehydrogenated or hydroxylated derivatives,⁶¹ as shown in **Equation 1.10**.



The hydroxyl radicals generated as a result of metabolic activities are scavenged by hydrogen peroxide molecules, resulting in the production of perhydroxyl radicals, as shown in **Equation 1.11**.



The generation of the hydroxyl free radical via the Fenton reaction and the overall Fenton process has been summarized in the above equations. In addition to ferrous ions, the ions of other transition metals can also be used to facilitate ROS generation by following Fenton-like reactions. However, ferrous ions are supposed to be the best suited for producing hydroxyl free radicals compared to ions of other transition metals.⁶²

In physiological conditions, copper ions possess greater solubility as compared to ions of iron. They can serve as a better catalyst for the Fenton reaction, but the iron ions are freely accessible in the biological system. The generated hydroxyl free radicals attack DNA molecules resulting in the strand breaking of the latter by abstracting a proton or adding a double bond.⁶³ The hydroxyl radicals target specific sites of DNA-base pairs, such as the C-8 site of guanine and adenine, which yields 8-hydroxydeoxyguanosine (8-OHdG) and 8 (or 4,5)-hydroxyadenine oxidation products.⁶⁴ DNA bases such as purine and pyrimidine are also prone to hydroxyl radical's attack, resulting in the formation of different intermediate products.⁶⁵

1.3 Detection of free radicals

Free radicals are highly reactive, and their reactivity imparts them with a short lifetime. The detection of such short-lived chemical moieties requires techniques that are fast, reliable, and sensitive. The half-lives of different ROS and RNS have been mentioned in **Table 1.1**, which serve as an indicator of high reactivity and least stability of free radicals.

Table 1.1 ROS and RNS produced during metabolic processes.⁶⁶

S. No.	Chemical Moieties	Symbolic representation	Half-life (s)
	ROS	-	-
1.	Alkoxy radical	RO•	10 ⁻⁶
2.	Hydroxyl radical	•OH	10 ⁻¹⁰
3.	Hydrogen peroxide	H ₂ O ₂	Stable
4.	Ozone	O ₃	1
5.	Peroxy radical	ROO•	17
6.	Singlet oxygen	¹ O ₂	10 ⁻⁶
7.	Superoxide anion radical	•O ₂ ⁻	10 ⁻⁶
	RNS	-	-
8.	Dinitrogen trioxide	N ₂ O ₃	1
9.	Nitric oxide	NO•	1
10.	Nitrogen dioxide	NO ₂ •	1
11.	Nitrous acid	HNO ₂	1
12.	Nitroxyl anion	NO ⁻	1
13.	Nitroxyl cation	NO ⁺	1
14.	Peroxy nitrite	ONOO ⁻	10 ⁻³

The methods employed for detecting free radicals have been classified into direct and indirect, as shown in **Figure 1.4**. These methods have been discussed in the subsequent sections.

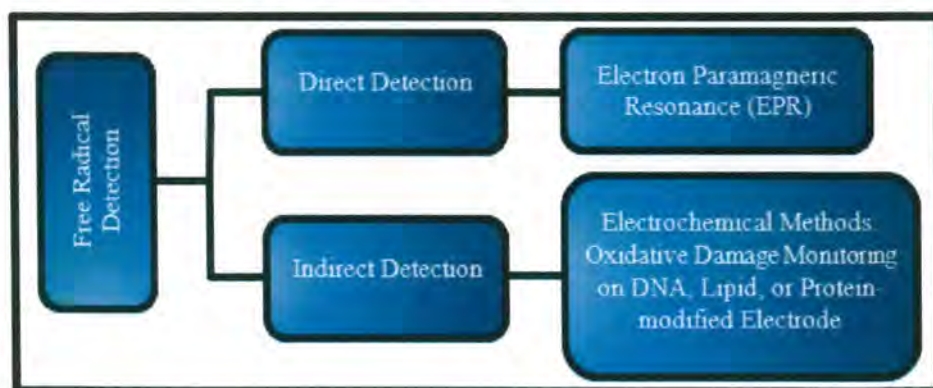


Figure 1.4 Methods for detection of free radicals.

1.3.1 Direct detection

The free radicals are directly detected by withdrawing a portion of the sample from the sources of free radicals, for example, during a biopsy and subjecting the withdrawn sample to a detection technique. Electron paramagnetic resonance spectroscopy (EPR) coupled with spin tracking is a commonly employed method for probing these highly short-lived chemical species consisting of unpaired electrons, such as hydroxyl radical (half-life = 10^{-10} s).⁶⁷ This technique requires a continuous supply of high concentrations of $\bullet\text{OH}$ to yield accurate results, which is not usually possible owing to changes in the free radical content due to their high reactivity.⁶⁸

1.3.2 Indirect detection

The indirect detection of free radicals is executed by using the principle of chemical derivatization coupled with a separation technique, such as high-performance liquid chromatography (HPLC) coupled with either mass spectrometry,⁶⁹ UV-Visible spectroscopy,⁷⁰ fluorescence method,⁷¹ or electrochemical detection (ED).⁷² HPLC coupled with ED facilitates the identification and quantification of $\bullet\text{OH}$ by monitoring the hydroxylation products generated as a result of a reaction between $\bullet\text{OH}$ and aromatic molecules.⁷³ Alike direct detection methods, these techniques also require a sampling procedure which reduces the reliability of the measurements.

Electrochemical methods facilitate the real-time detection (indirect) of free radicals by monitoring the oxidative damage of a modified electrode owing to the chemical interaction of the $\bullet\text{OH}$ free radical with the chemical moiety immobilized on the electrode's surface.⁷⁴ The DNA, lipids, and proteins are more prone to hydroxyl radical's attack in the biological system. Considering the high intrinsic affinity of $\bullet\text{OH}$ for the mentioned biological moieties, the monitoring of the oxidative damage of a DNA,⁷⁵ lipids,⁷⁶ or protein-modified electrode serves as an indicator for the presence of the mentioned free radical.⁷⁷

1.4 Sensors

Sensors are devices capable of facilitating the detection of any chemical, physical or electrical stimuli by converting the obtained information into a readable signal.⁷⁸ Sensors comprise a stimuli-sensitive recognition layer, a transducer, and a processor. The interaction of the analyte with the chemical moieties anchored at the surface of the sensing platform results in the generation of a signal. The signal is converted and forwarded by a transduction element to the processor. The processor amplifies and processes the signal to a readable form.⁷⁹

On the basis of their utility, sensors have been classified into the following categories, 1) biosensors, 2) physical sensors, and 3) chemical sensors.

1.4.1 Biosensors

The IUPAC system defines biosensors as self-contained integrated devices that generate quantitative or semi-quantitative information using a biological recognition layer that is retained in contact with a transduction element.⁸⁰ These sensors are sensitive to biochemical changes taking place in the living system. The obtained information is converted to an electrical signal by a transducer and subjected to amplification, followed by processing. Microbial potentiometric sensors and immunosensors are the most prominent type of biosensors.⁷⁸ Owing to their small size, low cost, quick results, and ease of use, they have applications in food processing, agriculture, pollution control, etc.⁸¹

1.4.2 Physical sensors

Physical sensors are devices that are sensitive to physical changes, such as temperature, sound, pressure, light, refractive index, absorbance, mass change, etc.⁸² The change in the physical parameters is detected by a micro-transduction element anchored to the tip of a probe. The signal is generated as a result of the analyte's ability to impart any physical change. The input signal of the physical stimulus determines the output signal. The generated signal's features depend on the transduction element's nature. The commonly used transduction elements for physical sensors include light-emitting resistors, surface acoustics, piezoelectrics, thermostats, etc.⁸³ Electrophysiological sensors, humidity sensors, pressure sensors, temperature sensors, etc., are common types of physical sensors.⁸⁴

1.4.3 Chemical sensors

These sensors represent a class of sensors that are sensitive to a specific chemical moiety present in a liquid or gaseous matrix. A chemical sensor is a device capable of transforming chemical information, such as the concentration of a specific sample component to the total composition of the sample obtained from the interaction between the analyte and the surface layer of the sensing scaffold, into an analytically useful signal.⁸⁵ Several compounds have been detected using these sensors owing to their rapid response. The working principle of these sensors involves the conversion of a chemical signal of the analyte species into an electrical, thermal or optical signal. The chemical sensors reveal the qualitative and quantitative information of the analyte.⁸⁶

The functioning of a chemical sensor is based on two units, namely, a receptor and a transducer. At times the receptor and the transducer are separated by a membrane.⁷⁸ In the receptor part, the information generated from the interaction between the analyte and chemical moieties immobilized on the sensor's surface is converted into a form that the transduction element can read. The transduction element converts the chemical information to an analytical signal.

The advancement in instrumentation, microelectronics, and computer technology has aided the fabrication of several sensors. Based on the working principle of the transduction element, the chemical sensors have been classified into different categories discussed in the subsequent sections.

1.4.3.1 Optical sensors

Optical sensors, also known as optodes, are devices sensitive to the variations in the optical phenomena arising due to the interaction of a specific chemical moiety, i.e., the analyte, with the receptor part of the sensor.⁸⁷ The variations in the optical phenomena include changes in absorbance, reflectance, refractive index, optothermal effects, etc. Optical fibers are configured in such types of sensors to facilitate their working, resulting in cost-effectiveness, miniaturized size, weight reduction, and prevention from electromagnetic interference.⁸⁸

1.4.3.2 Thermometric sensors

These sensors measure the heat effects of the analyte by monitoring specific chemical reactions. The changes in the heat effects, such as the heat of a combustion reaction, can be monitored using a thermistor.⁷⁸

1.4.3.3 Mass-sensitive sensors

These devices are sensitive to the mass changes at the surface of the recognition layer owing to the accumulation of the analyte. The change in the mass is governed by the extent to which a specific property of the recognition layer changes in response to the accretion of the analyte.⁸⁹ Piezoelectric devices facilitate the measurements made in response to the changes in a quartz plate's oscillation frequency owing to the analyte's deposition. The changes in the propagation velocity of an acoustic wave produced by the variation in the deposited mass of the analyte are monitored by surface acoustic wave devices.⁹⁰

1.4.3.4 Electrochemical sensors

These sensors can convert the electrochemical information generated due to the interactions between the analyte and the electrode into a readable signal.⁹¹ These interactions can be induced electrically or spontaneously at zero-current conditions.⁹² Electrochemical sensors are further classified into voltammetric sensors and potentiometric sensors.

In voltammetric sensors, the current response is determined in alternating (AC) or direct current (DC) mode. The electrodes used can be chemically inert, chemically active, or modified. Potentiometric sensors measure the potential of the indicator electrode, such as a redox electrode, against a reference electrode.

1.5 Protein immobilized polymer-modified electrodes

The detection of highly reactive and short-lived chemical moieties, such as free radicals, cannot be executed by ordinary electrodes. The monitoring of the oxidative damage of a DNA, lipid, or protein-modified electrode serves as a measure for the detection of free radicals. The innovative approach for detecting the hydroxyl radical involves immobilizing biological molecules, such as Bovine serum albumin (BSA), on the electrode's surface and subjecting it to hydroxyl free radical's attack.⁹³ The extent to which the immobilized protein is damaged is reflected in the electrochemical probe's current response, which indirectly serves as an indicator of the presence of the $\cdot\text{OH}$.⁹⁴ The earlier reported work suggests that the direct electron transfer (DET) between the immobilized BSA film and electrode is inconvenient and is a slow process.⁹⁵ Electron mediators or shuttles are required to be introduced before immobilizing protein on the electrode to aid a facile electron transfer process.

Thin films of conducting polymers, such as polypyrrole (PPy),⁹⁶ poly-o-phenylenediamine (PoPD),⁹⁷ polythiophene (PT),⁹⁸ polyindole (PIN),⁹⁹ polyaniline (PANI),¹⁰⁰ etc., obtained on the electrodes by electropolymerization of their respective monomers under optimized conditions exhibit a great potential to act as electrode modifying materials and facilitate a faster electron transfer. The poly-o-phenylenediamine modified electrode possesses electrostatic compatibility to promote BSA immobilization on its surface.

The immobilization of a protein on an electrode's surface requires it to be executed in such a way that the native structure, bioactivity, and stability of the protein should remain intact. The forthcoming sections discuss different strategies employed for anchoring and obtaining a consistent protein film on the surface of the polymer-modified electrodes.

1.5.1 Physisorption

This method involves the protein's adsorption on a substrate's surface. The Van der Waals forces of attraction promote the development of a stable protein film on the electrode's surface.¹⁰¹ The physically adsorbed protein film retains its structure and activity. However, the inability to offer long-term stability to the adsorbed film and the leaching of the protein limits the applicability of this method.

1.5.2 Chemisorption

This method involves the formation of a chemical linkage between the biological molecules, such as the protein and the electrode. The type of chemical linkage formed depends on the factors such as the properties of the electrode's surface, the nature of the biomolecule, and the crosslinker used. The protein film chemically adheres to the surface of the electrode following two (02) steps.¹⁰² The first step involves the activation of the substrate's surface using a chemical linker, followed by the second step, wherein the protein is allowed to assemble on the activated surface of the substrate. The chemically promoted adsorption of the protein on the electrode's surface is complex and imparts conformational changes that may affect the protein-modified electrode's working efficiency.

1.5.3 Film deposition

It is a smart approach that is employed to immobilize biomolecules on the surface of the electrode. Before anchoring the protein, the electrode's surface is modified using a polymer; this promotes the formation of a uniform protein film facilitated by the trapping of the biomolecules by the polymer.¹⁰³ Factors such as the nature of the polymer and the protein govern the electrostatic compatibility of the two, which leads to a uniformly anchored protein film on the polymer-modified electrode's surface.

1.6 Magnesium oxide (MgO)

It is a white crystalline solid that is hygroscopic in nature. Historically, it was referred to as magnesia alba.¹⁰⁴ Its chemical formula is MgO, and its lattice consists of Mg²⁺ and O²⁻ ions held together by a strong ionic bond. MgO serves as a source of magnesium. It does not occur naturally in the form of solid deposits owing to its tendency to slowly absorb moisture from the surrounding environment, which results in its conversion into magnesium hydroxide, which upon calcination yields MgO following the reaction shown in **Equation 1.12 and 1.13**.¹⁰⁵ Magnesium oxide is used as a heating substance due to its excellent thermal

conductivity. It is a poor electrical conductor owing to its high electrical resistivity. Some properties of bulk MgO have been listed in **Table 1.2**, given below.

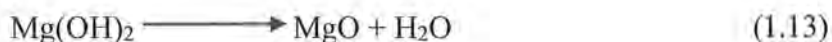
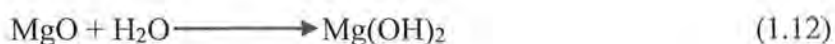


Table 1.2 Properties of MgO (bulk).¹⁰⁵

S. No.	Properties	
1.	Appearance	White
2.	Odor	Odorless
3.	Density	3.6 g/cm ³
4.	Crystal structure	Cubic
5.	Refractive index	1.735
6.	Dipole moment	6.2 ± 0.6 D
7.	Band gap	7.8 eV
8.	Thermal conductivity	45–60 W.m ⁻¹ .K ⁻¹
9.	Electrical resistivity	10 ¹⁶ Ω.m

In a lecture given at the annual meeting of the American Physical Society held at Caltech on December 29, 1959, physicist Richard Feynman suggested that “there’s plenty of room at the bottom”.¹⁰⁶ This establishes that when the bulk materials are brought to the nanoscale, they exhibit different properties compared to their bulk counterparts. Nanostructures include materials that have at least one of their dimension below 100 nm; this category includes materials with different morphologies, such as nanoparticles, nanospheres, nanorods, nanotubes, nanofilms, nanocubes, nanoflowers, etc.¹⁰⁷ The method employed for their synthesis and the resulting morphology collectively govern the applications for which they can be used. Owing to their dimensions in the nano range, nanomaterials exhibit phenomena like quantum confinement and phonon confinement.¹⁰⁸⁻¹⁰⁹ These phenomena facilitate the tuning of the nanomaterials’ electrical,¹¹⁰ magnetic,¹¹¹ optical,¹¹² thermal properties,¹¹³ etc.

Magnesium oxide nanostructures owing to the exhibition of several phenomena at the nanoscale have emerged as materials of scientific interest in the last two decades. Bulk MgO is considered as a highly insulating material due to its high optical band gap corresponding to 7.8 eV; however, its nanostructures, such as MgO nanoparticles of size less than 10 nm, exhibit

a modified optical band gap as low as 2.8 eV.¹¹⁴ One-dimensional MgO nanomaterial has been reported to exhibit a band gap of 3.2 eV.¹¹⁵ In addition to the variation in the optical band gap, the value of the dielectric constant increases when MgO is brought to the nanoscale.¹¹⁶ The phenomena exhibited by the MgO nanomaterials when they are brought into the nano regime have been highlighted in **Figure 1.5**.

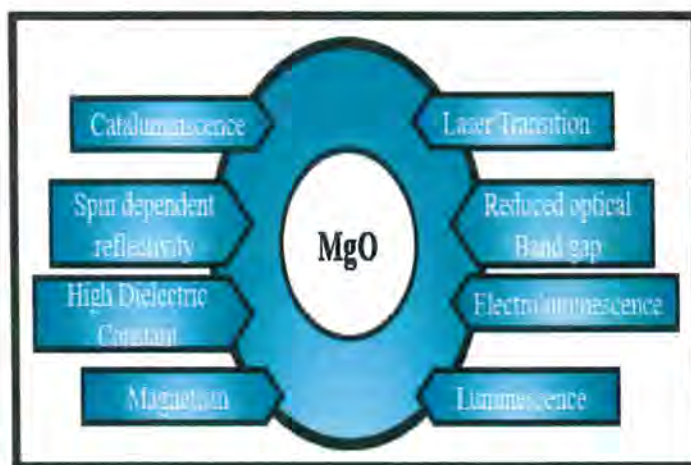


Figure 1.5 Phenomena exhibited by MgO at the nanoscale.¹¹⁷

The tailoring of the bulk magnesium oxide to the nanoscale imparts it with different phenomena and extends its utility for several applications. MgO nanostructures have been used in UV-photodetectors,¹¹⁸ degradation of dyes,¹¹⁹ removal of heavy metals from contaminated water,¹²⁰ precipitation of phosphorous and nitrogen from wastewater,¹²¹ low-field magnetic sensors,¹²² coating for cathodes and anodes of rechargeable batteries,¹²³ surfaces for promoting splitting of ethanol and methanol to produce hydrogen gas,¹²⁴ detection and degradation pesticides,¹²⁵ etc.

1.7 Literature review

The detection of hydroxyl free radical has been the main concern of the scientific world due to its deleterious effects on the working of a biological system. The methods proposed for its detection aimed to indicate the abnormal overproduction of $\bullet\text{OH}$ radical in a living system which can aid different pathological disorders appearing at later stages of life. Historically, the efforts to detect hydroxyl free radical date back to the 1980s. Initially, the proposed detection methods were based on chemical derivatization coupled with a separation technique and electrochemical detection (ED). After 2006, the focus shifted toward the electrochemical detection of hydroxyl free radical by monitoring oxidative damage.

(Slivka and Cohen, 1985) proposed a method based on generating hydroxyl free radicals in a dopamine-containing medium. The reaction of hydroxyl radical with dopamine resulted in the formation of three-ring monohydroxylated products, which were separated using high-pressure liquid chromatography (HPLC) and electrochemically examined using electrochemical techniques. The electrochemical signal of the formed products served as an indicator of the amount of hydroxyl free radical present in the medium.¹²⁶

(Floyd et al., 1986) proposed an efficient method based on HPLC coupled with ED. The DNA (2-deoxyguanosine) exposed to hydroxyl radicals was converted to 8-hydroxydeoxyguanosine (8-OHdG). The 8-OHdG was separated by employing HPLC and detected using ED. The electrochemical signal of 8-OHdG served as a measure for estimating its concentration, which indirectly established the concentration of $\cdot\text{OH}$ radical in the reaction medium.⁶⁴

(Feix and Kalyanaraman, 1991) fabricated a method based on electron spin resonance (ESR) and high-performance liquid chromatography trapping coupled with electrochemical detection. The hydroxyl free radical was produced during merocyanine 540 (MC 540) mediated photosensitization.¹²⁷

(Stemarie et al., 1996) designed a method to detect hydroxyl free radical by trapping it by 4-hydroxybenzoate using GC-MS and HPLC coupled with ED.¹²⁸

(Scholz et al., 2007) proposed an indirect method for the electrochemical detection of the hydroxyl free radical by monitoring the oxidative damage of self-assembled monolayers (SAM) of hexanethiol immobilized on metal electrodes measured from the current response of the redox couple $\text{Ru}^{2+}/\text{Ru}^{3+}$.⁷⁴

(Kato et al., 2011) described the fabrication of a nanocarbon film electrode for the electrochemical determination of the oxidative damage imparted to DNA by hydroxyl radical. The extent of oxidative damage served as a measure of quantification of the hydroxyl radical present in the medium.¹²⁹

(Bian et al., 2011) proposed a sensitive electrochemical probe for the detection of hydroxyl free radical based on bovine serum albumin immobilized poly-*o*-phenylenediamine anchored carbon-coated nickel nanocomposite-modified glassy carbon electrode.¹³⁰

(Jabeen et al., 2017) fabricated an electrochemical probing platform for monitoring hydroxyl free radicals based on flavonoid-modified APTES-FTO electrodes.¹³¹

(Wang et al., 2018) designed an electrochemical sensor to detect hydroxyl free radicals based on 4-hydroxybenzoic acid (4-HBA) modified glassy carbon electrode. The $\bullet\text{OH}$ radicals were trapped by 4-HBA, and this resulted in the generation of electroactive 3,4-dihydroxybenzoic acid (3,4-DHBA), whose electrochemical signal served as a measure of the concentration of $\bullet\text{OH}$.¹³²

(Huang et al., 2019) proposed a biosensor based on a modified glassy carbon electrode to detect the hydroxyl radical. The designed sensing platform consisted of a layer of nitrogen-doped porous carbon material, electrodeposited gold nanoparticles (AuNPs), and a film of thiolated DNA immobilized on the electrode's surface using Au-S bonds.⁷²

(Duanghathaipornsuk et al., 2020) fabricated a composite sensor by immobilizing a layer of prussian blue (PB) dye and a nanocomposite composed of cerium oxide nanoparticles and graphene oxide on a GCE. The hydroxyl free radicals generated via the Fenton reaction oxidized Ce^{3+} to Ce^{4+} and the electrochemical signal generated served as a measure of the concentration of $\bullet\text{OH}$ free radical.⁶⁸

(Duanghathaipornsuk et al., 2021) designed a sensitive electrochemical sensing scaffold based on a composite of ultra-small cerium oxide nanoclusters grafted on a conducting carbonaceous material deposited on a screen-printed carbon electrode for the in vitro detection of hydroxyl free radical.¹³³

Considering the literature survey mentioned above and the complexities associated with the detection of hydroxyl free radicals, scientists have made valuable contributions. Still, they had shortcomings regarding selective, sensitive, and real-time detection of hydroxyl free radicals. The electrochemical probing platform proposed in this work is based on BSA-immobilized PoPD-anchored MgO-modified CPE. The designed sensor exhibited high stability and selectivity for real-time detection of hydroxyl radicals in the Fenton system.

1.8 Aim of work

An immense amount of work has been done to detect relatively long-lived superoxide anion radical and hydrogen peroxide in either vitro or vivo using different techniques. However, inconsiderable attention has been paid to the real-time detection of highly reactive and short-lived hydroxyl radicals owing to the unavailability of an efficient, selective, and specific technique. The aims of this project are set as follows:

- To develop a reliable and reproducible chemical system for the indirect detection of the •OH radical.
- To synthesize a suitable metal oxide nanomaterial that can act as a stable substrate in the chemical environment consisting of •OH radical.
- To incorporate the synthesized nanomaterial in fabrication of a CPE and use that as an active electrode for the voltammetric detection of the •OH radical.
- To investigate the resultant modified electrode as an electrochemical probe for •OH detection.

The aims mentioned above were achieved through following route.

The current research features a protein-based electrochemical sensor to facilitate the timely and reliable detection of hydroxyl free radicals. The earlier reported works suggest that the rate of electron transfer between the protein (bovine serum albumin) and the electrode is sluggish; this was eradicated by introducing a thin film of poly-o-phenylenediamine on the surface of the electrode, which was supposed to act as an electron mediator or shuttle between the two. The pre-existing literature establishes that the protein is poorly retained on the commercially acquired glassy carbon electrode (GCE) due to the peeling of the former; this was eliminated by fabricating carbon paste electrodes (CPEs). Nanostructures are materials that exhibit unique properties, and owing to this, undoped and Zn^{2+} doped MgO nanomaterials were synthesized. The synthesized nanomaterials were used for fabricating MgO-based CPEs. The proposed MgO nanomaterial-based protein immobilized polymer-modified electrode was used for the voltammetric detection of hydroxyl free radicals generated in the Fenton system.

CHAPTER 02

EXPERIMENTAL

This chapter highlights all the experimental work performed during this research work. It includes information about the chemicals used, instruments employed, and details of different synthetic and analytical tasks carried out systematically.

2.1 Chemicals and reagents

The chemicals and reagents which facilitated this research are mentioned in Table 2.1, along with their specifications. Deionized water with a resistivity ranging from 12 M Ω to 18 M Ω was utilized to prepare all the required solutions.

Table 2.1 The chemicals/reagents and their specifications.

S. No.	Chemicals/Reagents	Percentage purity (mass %)	Supplier
1.	Acetone	99	Sigma-Aldrich
2.	Bovine serum albumin	$\geq 95-98$	Sigma-Aldrich
3.	Ethanol	99	BDH
4.	Ethylene glycol	99	Merck
5.	Graphite powder	99	Sigma-Aldrich
6.	Hydrochloric acid	37	Sigma-Aldrich
7.	Hydrogen peroxide	35	BDH
8.	Iron (II) sulfate heptahydrate	≥ 99	Sigma-Aldrich
9.	Magnesium nitrate hexahydrate	≥ 99	Sigma-Aldrich
10.	Methyl violet	≥ 88	Merck
11.	Nitric acid	65	Sigma-Aldrich
12.	o-Phenylenediamine	≥ 99	Merck
13.	Paraffin oil	-	Sigma-Aldrich
14.	Potassium chloride	≥ 99	Merck
15.	Potassium hexacyanoferrate	≥ 99	Sigma-Aldrich
16.	Sodium dihydrogen phosphate monohydrate	≥ 99	Merck
17.	Sodium dodecyl sulfate	≥ 99	Sigma-Aldrich

18.	di-Sodium hydrogen phosphate dihydrate	≥ 99	Merck
19.	Sulfuric acid	$\geq 95-97$	Sigma-Aldrich
20.	Zinc nitrate hexahydrate	98	Sigma-Aldrich

2.2 Instrumentation

This section includes the details of all the instruments used during the experimental part of this research work.

2.2.1 Electrochemical workstation

All the electrochemical experiments, i.e., cyclic voltammetry, square wave voltammetry, and electrochemical impedance spectroscopy, were conducted on a Gamry Interface 1000E Potentiostat (Louis Drive Warminster, PA 18974, USA) equipped with Gamry Framework version 7.05 and Gamry Analyst version 7.05 software. The Gamry potentiostat model 1000E is an advance electrochemical workstation that is capable of working efficiently in both the potential control range (± 1 mV, $\pm 0.2\%$ of setting and reading) and the current control range (± 5 pA, $\pm 0.3\%$ of range).



Figure 2.1 Electrochemical workstation connected with a voltammetric cell.

The voltammetric cell used during this research work is depicted in **Figure 2.1**. The cell was a 20mL glass vial with a Teflon cap having three (03) standard taper ports for inserting the electrodes within the cell. All voltammetric experimentations were conducted using a three-electrode system. The three-electrode system consisted of a commercially available glassy carbon electrode (GCE) with an area of 0.0707 cm^2 or a fabricated carbon paste electrode

(CPE), a platinum (Pt) wire, and a saturated calomel electrode (SCE, +0.241 V vs. SHE), serving as working electrode, auxiliary electrode, and reference electrode respectively.

The reaction of interest takes place on the working electrode. Depending on the potential applied, it can function as a cathode or an anode. The working electrode's potential is varied with respect to the reference electrode. The counter electrode completes the circuit, and a reaction opposite to the one on the working electrode occurs here. A minimum distance was maintained between the working and the reference electrode to minimize the ohmic drop or IR drop effect.¹³⁴ This ensures that the current measurement on the working electrode is free from fluctuations taking place at the counter electrode.

2.2.2 UV-Visible spectrometer

The UV-Visible spectroscopic technique was employed to evaluate the optical properties of methyl violet (MV) dye. The UV-Visible spectroscopic measurements were facilitated by Shimadzu spectrophotometer model 1700. The UV-Visible radiations were generated using deuterium and tungsten lamps in the spectrophotometer. The absorption spectra were recorded in the wavelength ranging from 400-800 nm. Depending on the wavelength of the radiation and the gap between HOMO and LUMO, different electronic transitions occur within the analyte.¹³⁵ Shimadzu 1700 is a double beam spectrophotometer; this suggests that the reference and the sample cell can be exposed to two beams of light. Quartz cells of 1 cm path length were used during the spectroscopic measurements. The absorption spectra of methyl violet were monitored and served as an indicator for the presence of the hydroxyl free radical ($\cdot\text{OH}$) within the system under investigation.

2.2.3 X-ray diffraction (XRD) analysis

It has the capability to serve as a powerful tool for identifying crystalline or semi-crystalline materials. The X-ray diffraction patterns of synthesized materials are compared with the standard X-ray diffractograms obtained from their respective JCPDS (Joint committee on powder diffraction standards) cards available in the ICDD (International center for diffraction data) database. In addition to identification, the XRD analysis also reveals information related to the phase, crystal orientation, structure, and structure-related parameters such as average crystallite size, defects, and strain.¹³⁶

The synthesized undoped MgO and Zn^{2+} doped MgO nanomaterials were characterized using PANalytical X-ray diffractometer model 3040/60 X'Pert PRO operated at 45 kV and 40 mA. Copper's $\text{K}\alpha$ radiation ($\lambda=0.154$ nm) served as X-ray radiation applied at a step size of

0.025° over 2θ values ranging from 10°-80°. A finely powdered form of MgO nanomaterials was subjected to XRD analysis, and the obtained results were used to determine the average crystallite size using the formula shown in **Equation 2.1**.

$$D = \frac{k\lambda}{\beta \cos\theta} \quad (2.1)$$

The formula represented in **Equation 2.1** is the Debye-Scherrer formula, where D represents the size of the crystallite, k is the Scherrer's constant, λ denotes the wavelength of the incident X-ray radiation, β represents the full width at half maximum (FWHM) of the diffraction peak in radians, and θ is the Bragg's diffraction angle.

The value of Scherrer's constant (k) is either taken as 0.9 or 1, depending on the morphology of the crystallites (0.9 for spherical).¹³⁷ The wavelength of incident X-ray radiation (λ) in the case of copper's $K\alpha$ is 0.154 nm.

2.2.4 Scanning electron microscope coupled with Energy dispersive x-ray spectroscopy (SEM+EDX)

Scanning Electron Microscopy is a versatile tool for investigating nanomaterials' microstructure, morphology, and size. SEM coupled with EDX facilitates the chemical composition characterization of the sample by revealing its elemental composition.¹³⁸

The SEM micrographs and the elemental map of synthesized undoped MgO nanomaterial were obtained using Nova Nano SEM 450 Field-Emission Scanning Electron Microscope (FESEM). It provides high resolution up to 1.4 nm in high vacuum mode under a low voltage of 1 kV with an added EDX capability.

2.3 Experimental procedure

This section includes the method employed for synthesizing MgO nanomaterials, the procedure adopted for fabricating the electrodes, and the modification of the fabricated electrodes.

2.3.1 Synthesis of MgO nanomaterials

In the present work, undoped and Zn^{2+} doped MgO nanomaterials were synthesized by employing the fuel/solvent combustion method following an earlier reported work.¹³⁹ The fuel combustion method is simple, fast, and cost-effective.

The undoped MgO nanomaterial was synthesized by adding 1.2 g of magnesium nitrate hexahydrate ($Mg(NO_3)_2 \cdot 6H_2O$) to 10mL of ethylene glycol ($C_2H_6O_2$), which served as a fuel.

The reaction mixture was stirred for 1 hour using a magnetic stirring bar at ambient temperature. The reaction mixture was then transferred to a china dish, which was then placed in an oven for 1 hour at a temperature of 200 °C. When the fuel (solvent) had combusted, the dried contents of the reaction mixture were subjected to calcination for 2 hours at a temperature of 500 °C.

The zinc-doped magnesium oxide (Zn^{2+} doped MgO) nanomaterials were synthesized by adding 2, 4, 6, 8, or 10 wt.% of zinc nitrate hexahydrate ($\text{Zn}(\text{NO}_3)_2 \cdot 6\text{H}_2\text{O}$) along with 1.2 g of magnesium nitrate hexahydrate to 10mL of ethylene glycol followed by employing the same procedure stated above. The synthesis of undoped MgO and Zn^{2+} MgO has been portrayed in **Figure 2.2**.

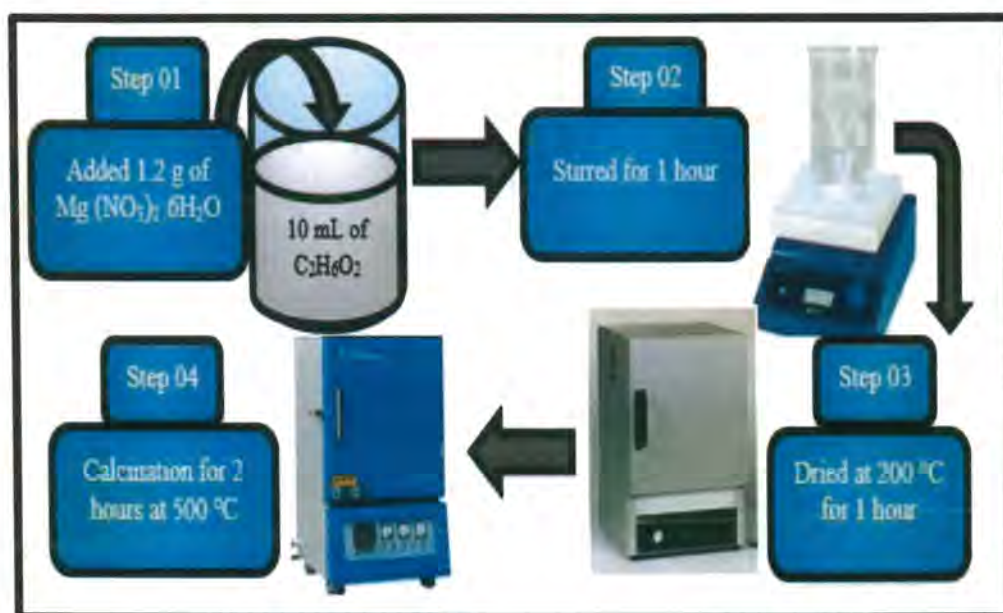


Figure 2.2 Pictorial representation of the synthesis of MgO nanomaterials.

2.3.2 Fabrication of the electrodes

This section highlights the procedure adopted for fabricating the electrodes and the method employed to ensure a cleaner and smoother (consistent) electrode surface.

2.3.2.1 Activation of graphite

Graphite was pretreated before the electrode fabrication to ensure that it was free from organic and inorganic impurities. The graphite was pretreated by following the standard procedure.¹⁴⁰ A weighed amount of graphite was cleaned with acetone and activated using aqua regia for 30 minutes followed by drying. After this treatment, the dried graphite powder was

washed with distilled water and then subjected to heat treatment for 4 hours at a temperature of 400 °C.

2.3.2.2 Fabrication of carbon paste electrodes (CPEs)

They are easy to make and cost-effective electrodes. Their key benefits include simple design, ease of modification, low background current, regeneration of the surface layer, negligible ohmic resistance, and electro-inactivity over a wide potential range. Carbon paste is a binary mixture of a carbon-based component, preferably graphite, and an organic liquid of non-electrolytic character, such as paraffin oils forced in glass, PVC, or Teflon® tubes.¹⁴¹

For fabricating bare CPE, 0.5 g of pretreated graphite was weighed and transferred to a china dish; this was followed by adding 0.3 mL of paraffin oil, which resulted in the formation of a homogenized paste. A portion of the homogenized paste was forced into a Teflon® tube of an inner diameter of 3 mm and a length of 5 cm. When the paste in the tube dried, a copper wire was inserted from the opposite end of the tube in the back of the mixture to establish electrical contact.

The synthesized undoped MgO and Zn²⁺ doped MgO nanomaterials were used to fabricate MgO-based carbon paste electrodes (MgO/CPE); this was done by adding 0.04 g of the synthesized nanomaterial to 0.46 g of graphite, then 0.3 mL of paraffin oil was added. The formed paste was pressed into a Teflon® tube, and a copper wire was inserted to establish electrical contact. The fabrication of bare and MgO-based carbon paste electrodes has been pictorially depicted in **Figure 2.3**.

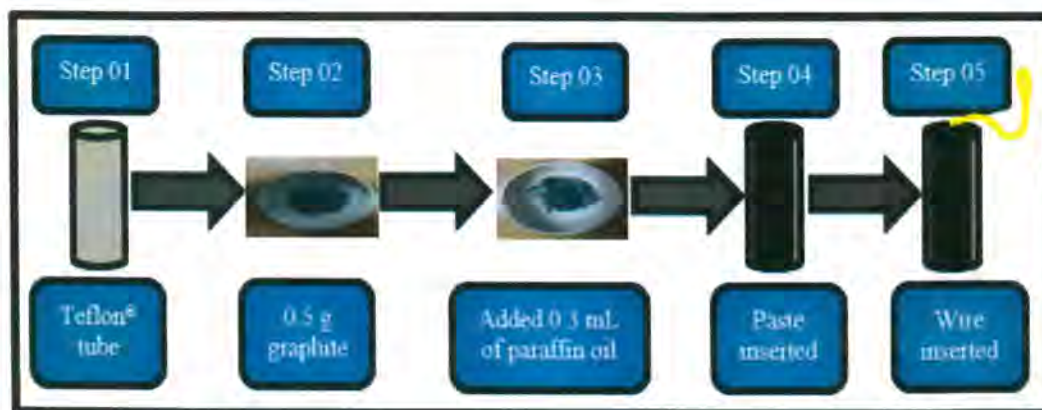


Figure 2.3 Pictorial illustration of the electrode fabrication process.

In total, seven (07) CPEs were fabricated. These consisted of a bare CPE and six (06) MgO-based CPE. Out of those six (06) MgO-based CPEs, one (01) was fabricated from

undoped MgO, and the rest of five (05) were fabricated from Zn²⁺ doped MgO, differing from one another on the basis of the loading (wt.%) of Zn²⁺ in the MgO nanomaterials. The fabricated electrodes are shown in **Figure 2.4**.



Figure 2.4 The fabricated carbon paste electrodes (CPEs).

2.3.2.3 Physical cleaning of the electrodes

To achieve reliable and accurate results during electrochemical analysis, it was ensured that the GCE's and the CPE's surface was clean and free from any grooves.¹⁴² This was done by polishing GCE on a nylon cleaning pad containing alumina-water slurry (0.05 μm). The electrode was polished by rubbing its surface on a nylon cleaning pad in a fashion of digit 8, then rinsed with distilled water. To obtain a clean and smooth (consistent) surface, the CPEs were rubbed on sandpaper, followed by rinsing with ethanol and a jet of distilled water.

2.3.3 Surface modification of the fabricated electrodes

To improve the efficiency and selectivity of the fabricated CPEs and commercially acquired GCE were subjected to different surface modifications to facilitate faster electron transfer kinetics. These modifications have been discussed in the sub-sections given below.

2.3.3.1 Electropolymerization of *o*-phenylenediamine

The fabricated electrodes were to be employed to indirectly detect hydroxyl radical by monitoring the oxidative damage on a protein immobilized electrode. The rate of electron transfer between the protein and the electrode is sluggish; this hinders the applicability of the designed sensing platform for the above-mentioned purpose.¹³⁰ The functionalization of the

electrode's surface using a mediator or a shuttle before anchoring the protein can facilitate a facile transfer of the electrons between the protein and the electrode.

o-Phenylenediamine (o-PD) is a monomer that upon electrochemical or chemical oxidation, yields a semi-conducting polymer known as poly-o-phenylenediamine (PoPD).¹⁴³ The thin PoPD film formed at the surface has been used for different applications, such as electron-transfer facilitator, electrochemical diode, pH sensors, and corrosion protection of metals.¹⁴⁴

o-PD was electropolymerized on the surface of the GCE and fabricated CPEs following an already reported procedure.¹³⁰ The working electrode, along with a reference electrode (SCE) and counter electrode (Pt wire), was inserted in a voltammetric cell containing a 0.5 mM solution of o-PD in 0.5 M sulfuric acid (H_2SO_4), which acted as a supporting electrolyte. Gamry electrochemical workstation equipped with Gamry Framework 6.03 software facilitated the electropolymerization of o-PD by employing the cyclic voltammetric technique in the potential window ranging from -0.6 V to $+1.2$ V for six (06) consecutive scans at a scan rate of 100 mV/s. A sharp oxidation peak that appeared at a potential of 0.613 V served as an indicator of the polymerization process. After the completion of the cyclic voltammetric analysis, the electrode was removed from the cell and rinsed with phosphate buffer saline (PBS) (pH=5.2) to remove any unanchored o-PD from its surface. The cyclic voltammogram obtained as a result of electropolymerization of o-PD is shown in **Figure 2.5**. The electropolymerization process has been pictorially illustrated in **Figure 2.6**.

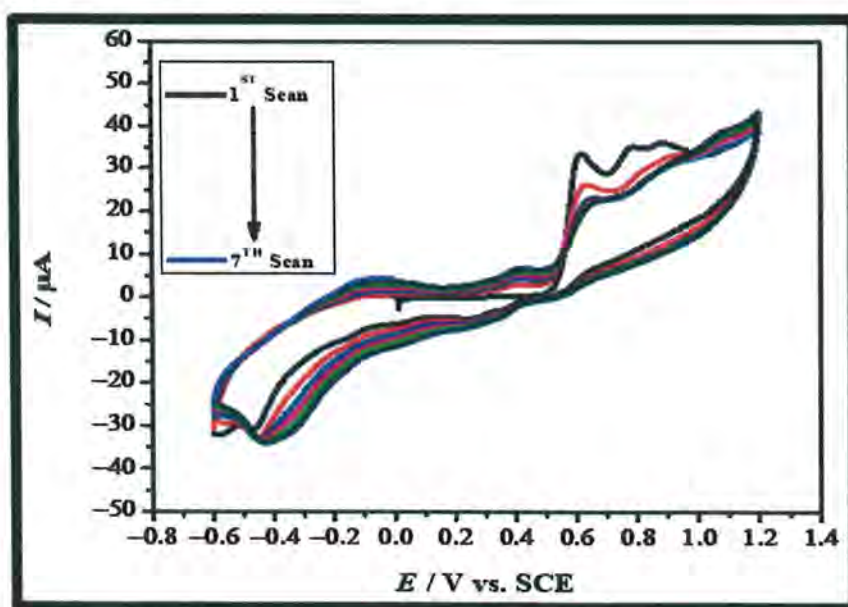


Figure 2.5 Cyclic voltammograms of six consecutive scans obtained for electropolymerization.

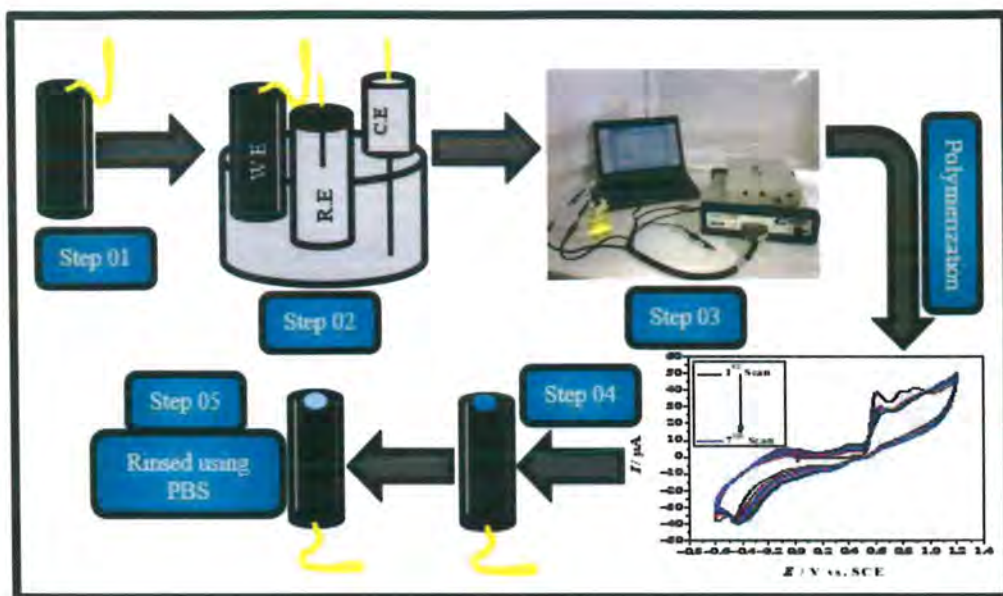


Figure 2.6 Pictorial illustration of the electropolymerization of *o*-PD.

The square wave voltammetric response of the PoPD-modified electrodes was recorded in the potential window ranging from 0 V to -0.8 V in PBS (pH=7).

2.3.3.2 Immobilization of Bovine serum albumin (BSA)

The polymer-modified electrode was subjected to protein immobilization by placing it in a solution (0.01 M) of BSA (protein) for half an hour. The protein was immobilized on the polymer-modified electrode's surface owing to the electrostatic force of attraction existing between the polymer and the protein. The electrode was removed and washed with 2% sodium dodecyl sulfate (SDS) solution and rinsed with distilled water. The protein immobilization process is pictorially illustrated in **Figure 2.7 and 2.8**.

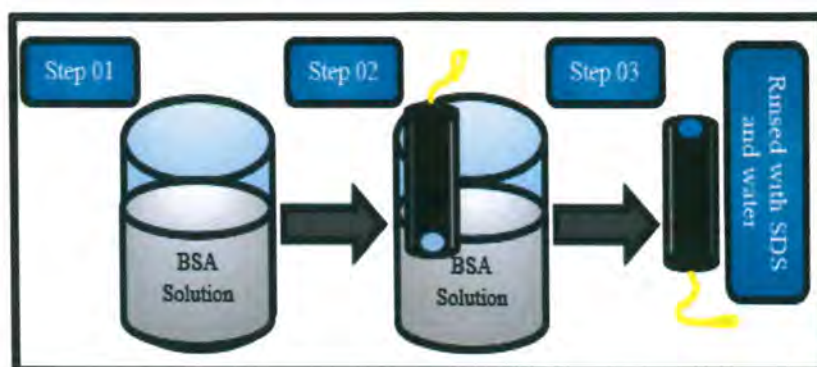


Figure 2.7 Pictorial illustration of the process of immobilizing BSA on PoPD-modified electrodes.



Figure 2.8 BSA immobilization on PoPD-modified electrodes.

The square wave voltammetric response of the protein immobilized polymer-modified electrodes was recorded in the potential window ranging from 0 V to -0.8 V in PBS (pH=7).

2.4 Electrochemical detection of hydroxyl radical on the designed sensing platform

The proposed sensing platform was placed in a medium consisting of the hydroxyl free radical to evaluate the practical utility of detecting the hydroxyl free radical. The generation of hydroxyl free radical was mimicked using the Fenton reaction. The protein immobilized polymer-modified electrode was placed in PBS (pH=7) solution consisting of 10 mL of 45 mM solution of H_2O_2 and 10 mL of 12 mM solution of Fe^{2+} for 30 minutes under constant stirring. After the passage of 30 minutes, the electrode was removed. The process of the hydroxyl free radical's attack on the electrode placed in the Fenton system is depicted in **Figure 2.9** and **2.10**.

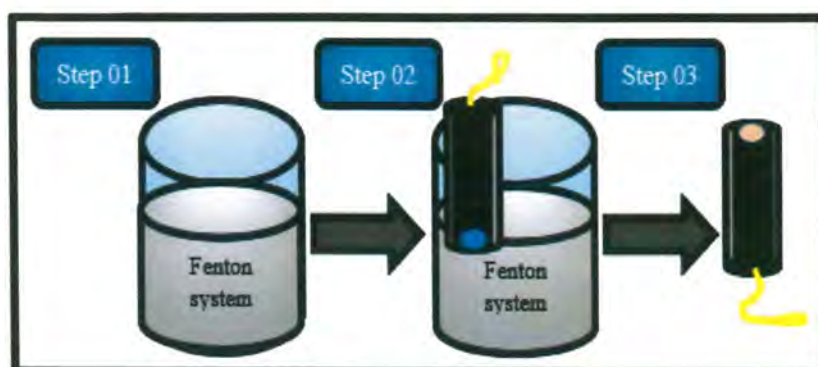


Figure 2.9 Pictorial illustration of the Hydroxyl attack on the BSA immobilized PoPD-modified electrodes.



Figure 2.10 *Hydroxyl free radical attack on BSA immobilized PoPD modified electrodes.*

The square wave voltammetric response of the protein immobilized polymer-modified electrodes was recorded in the potential window ranging from 0 V to -0.8 V in PBS (pH=7) after the hydroxyl free radical attack.

CHAPTER 03

RESULTS AND DISCUSSION

This chapter contains a detailed discussion of the results obtained from the experimental work conducted during this research.

3.1 Characterization of the synthesized nanomaterials

The undoped MgO and Zn²⁺ doped MgO nanomaterials were qualitatively analyzed using the X-ray diffraction (XRD) technique and Energy dispersive x-ray spectroscopy (EDX). Scanning electron microscopy served as a useful tool for determining their morphology and size.

3.1.1 X-ray diffraction analysis

The undoped and Zn²⁺ doped MgO nanomaterials were subjected to X-ray diffraction analysis. The X-ray diffractograms of the synthesized nanomaterials were in agreement with the standard XRD pattern of MgO obtained from its JCPDS Card No. 78-0430, available in the ICDD database. The X-ray diffractograms of the synthesized nanomaterials have been exhibited in **Figure 3.1**.

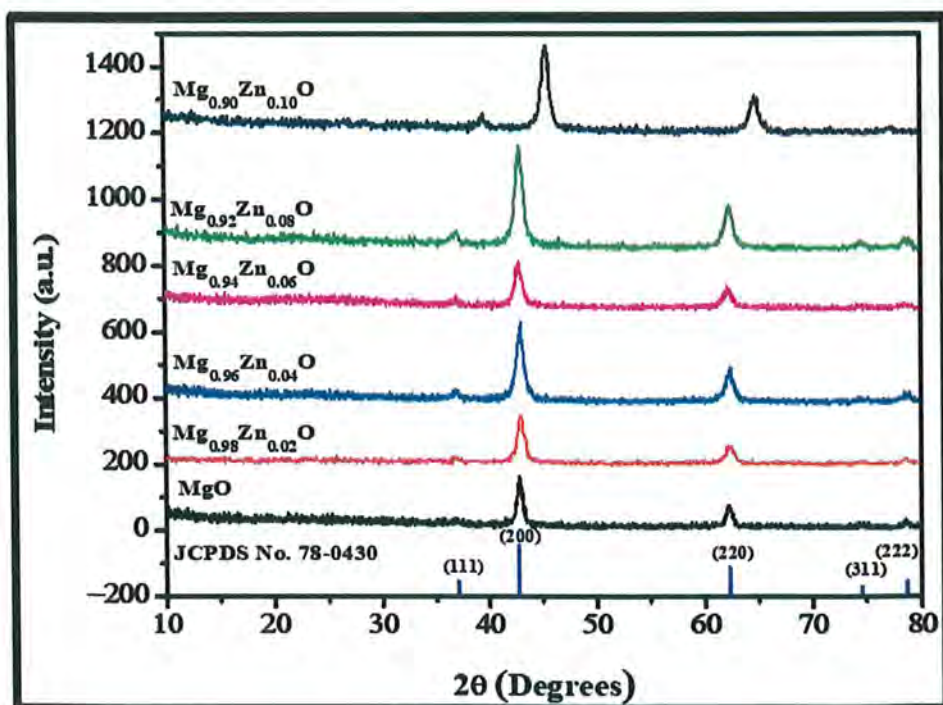


Figure 3.1 XRD patterns of synthesized undoped MgO and Zn²⁺ doped MgO along with standard pattern obtained from JCPDS card no. 78-0430.

The peaks positioned at 2θ values 36.9° , 42.8° , 62.2° , 74.5° , and 78.6° were indexed as (111), (200), (220), (311), and (222), respectively. The X-ray diffractogram of synthesized undoped MgO was in complete agreement with the standard XRD pattern of MgO. In comparison to the undoped MgO, Zn^{2+} doped MgO exhibited shifts in the peak position, peak broadening, and greater peak intensity which served as an indicator of successful doping of Zn^{2+} in the lattice of MgO.

The X-ray diffractograms of Zn^{2+} doped MgO shown in **Figure 3.1** suggest that the doping of Zn^{2+} in MgO resulted in the generation of a strain in the lattice of MgO, this type of strain is known as microstrain. The microstrain is further classified into homogenous microstrain and inhomogeneous microstrain. The inhomogeneous microstrain results in peak broadening, whereas a homogenous microstrain shifts the XRD peak's position. In comparison to undoped nanomaterial, peak broadening was observed in the XRD peaks of $Mg_{0.98}Zn_{0.02}O$, $Mg_{0.96}Zn_{0.04}O$, $Mg_{0.94}Zn_{0.06}O$, and $Mg_{0.92}Zn_{0.08}O$ nanomaterials which served as an indicator of the presence of an inhomogeneous microstrain within the lattices of these nanomaterials. The $Mg_{0.90}Zn_{0.10}O$ nanomaterial exhibited shifts in the XRD peak positions, suggesting that this nanomaterial possessed a homogenous microstrain within its lattice.

The intensity of the XRD peaks depends on the structure factor (F), which is related to the position of the atoms/ions within the lattice. The structure factor depends on the atomic scattering factor (f). It denotes the ratio of the amplitude of the X-rays scattered by a given atom and those scattered by an electron. The value of f depends on the nature of the atom. The introduction of the dopant Zn^{2+} in the lattice of MgO results in a slight change in the atomic scattering factor and affects the position of the particles within the lattice, which results in a variation in the structure factor. In comparison to the XRD peaks of undoped MgO, the XRD peaks of Zn^{2+} doped MgO exhibited greater intensity due to changes in the atomic scattering factor and structure factor.

The average crystallite sizes of the synthesized undoped and zinc-doped magnesium oxide nanomaterials were determined using the Debye-Scherrer formula (**Equation 2.1**). The calculated crystallite sizes have been shown in **Table 3.1**. The effect of doping Zn^{2+} in the lattice of MgO is also evident from the calculated crystallite sizes. The crystallites of the undoped MgO nanomaterial had the greatest size, whereas those of Zn^{2+} doped MgO were smaller.

Table 3.1 Average crystallite sizes of synthesized nanomaterials.

S. No.	Sample	The average crystallite size (nm) ± 1 nm	
		(200)	(220)
1.	MgO	25	22
2.	Mg _{0.98} Zn _{0.02} O	14	9
3.	Mg _{0.96} Zn _{0.04} O	9	11
4.	Mg _{0.94} Zn _{0.06} O	14	15
5.	Mg _{0.92} Zn _{0.08} O	20	12
6.	Mg _{0.90} Zn _{0.10} O	12	11

3.1.2 Scanning electron microscopy and Energy dispersive X-ray spectroscopy

Scanning electron microscopy (SEM) was employed to investigate the morphology and size of the synthesized MgO nanomaterial. The SEM micrographs of MgO nanomaterial have been depicted in **Figure 3.2 (A and B)**.

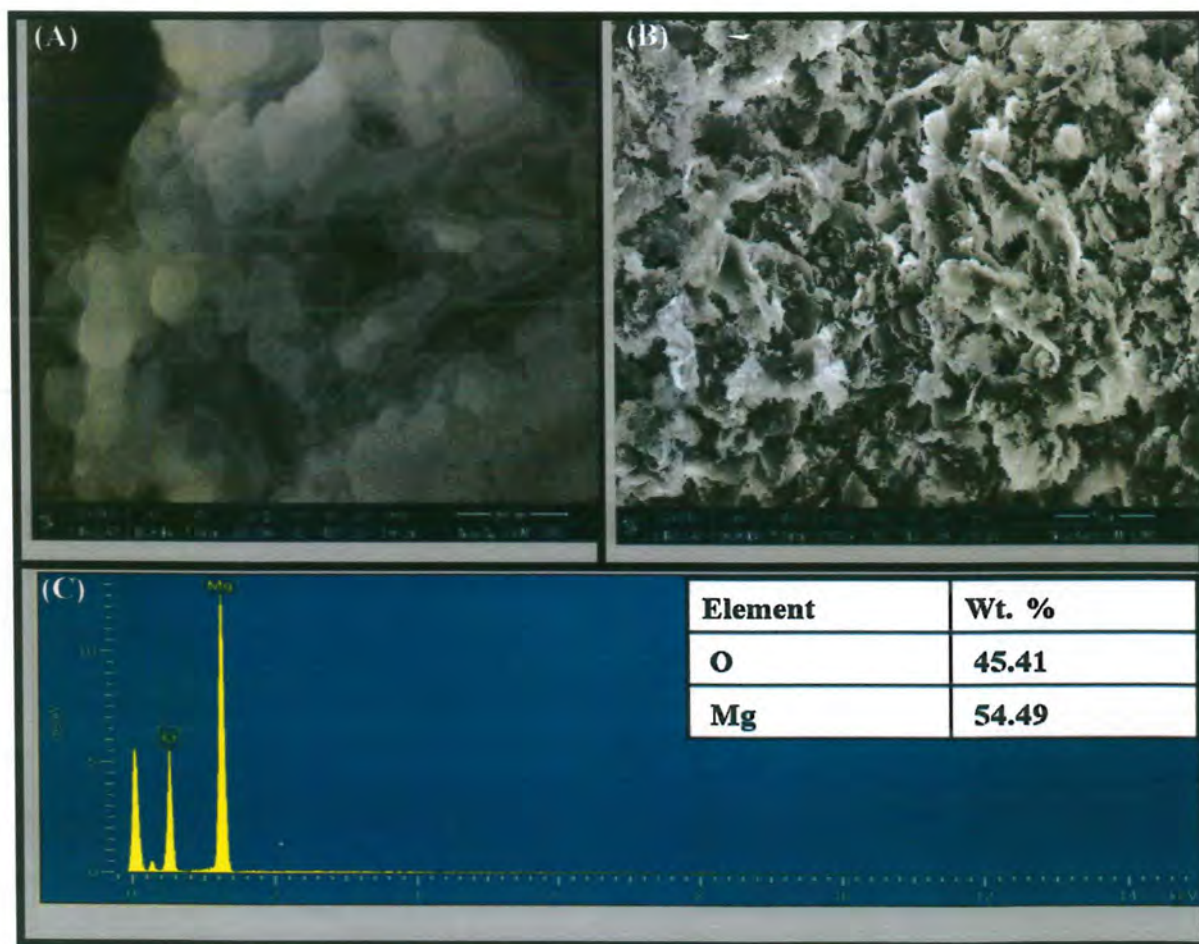


Figure 3.2 (A, B) SEM micrographs and (C) EDX spectrum of synthesized MgO nanomaterial.

The SEM micrographs reveal that the synthesized MgO nanomaterial was agglomerated, and the particle size was between 70 to 90 nm. In high-resolution **Figure 3.2 (A)**, hexagon-shaped particles are evident, and in low-resolution **Figure 3.2 (B)**, homogeneous thick flakes are present. The EDX spectrum of the MgO nanomaterial depicted in **Figure 3.2 (C)** suggests that the synthesized nanomaterial was free from impurities, and only magnesium and oxygen were present.

3.2 UV-Visible spectroscopic analysis

Ultraviolet-Visible (UV-Vis) spectroscopy, owing to its simplicity and availability in common labs, was employed to investigate the generation of hydroxyl free radical ($\bullet\text{OH}$) in the Fenton system. Another method, such as Electron paramagnetic resonance (EPR) spectroscopy coupled with spin tracking, is a common approach for directly detecting hydroxyl free radicals. In this work, the absorption spectra of methyl violet (MV) dye were recorded in the absence and presence of the solutions of hydrogen peroxide (H_2O_2) and ferrous (Fe^{2+}) salt to account for the presence of hydroxyl radical in the Fenton system.

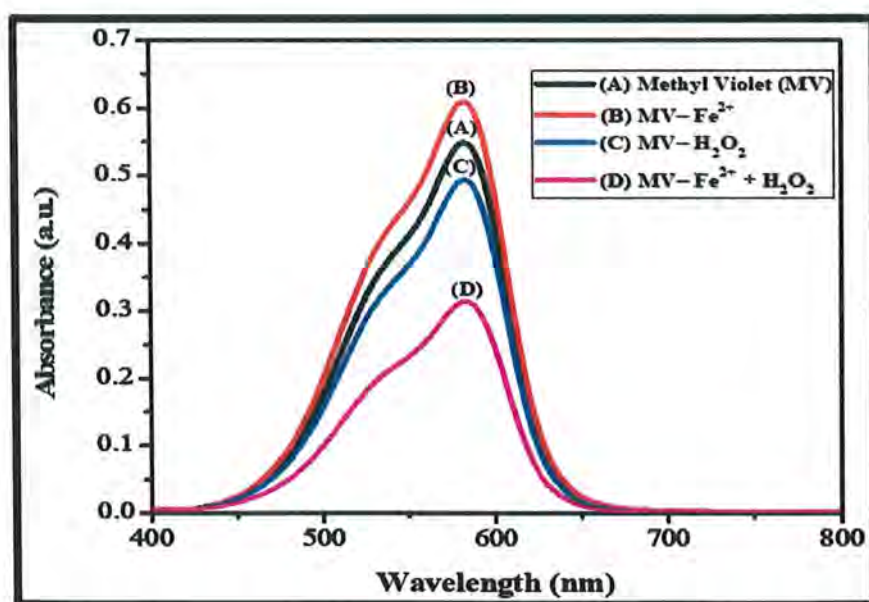
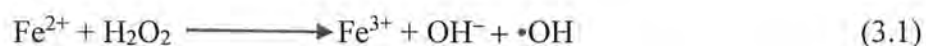


Figure 3.3 UV-Vis spectrum of (A) methyl violet (MV), (B) $\text{MV} + \text{Fe}^{2+}$, (C) $\text{MV} + \text{H}_2\text{O}_2$, and (D) $\text{MV} + \text{H}_2\text{O}_2 + \text{Fe}^{2+}$, with concentration MV 0.06 mM, Fe^{2+} 12 mM, and H_2O_2 45 mM respectively.

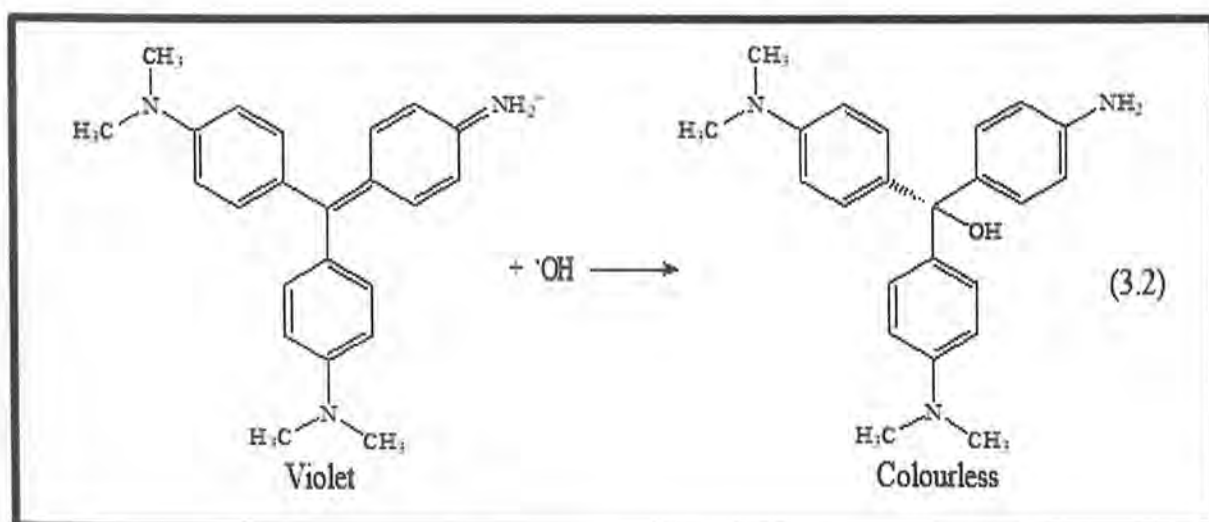
The blank reading of the deionized water (solvent) was also obtained to ensure that the obtained UV-Visible spectra of MV dye were free from any interference of the medium.

The spectra of MV dye have been depicted in **Figure 3.3**. The absorption spectrum of methyl violet dye (**A**) exhibits a clear absorption at 583 nm, which agrees with earlier reported work.¹⁴⁵ It appears that when the solution of the ferrous ions was added to the solution of methyl violet, a complex (MV-Fe²⁺) might have formed between the two resulting in increased absorption of light (hyperchromic shift) as shown in the spectrum (**B**). On the contrary, a hypochromic shift was observed in the case when the solution of hydrogen peroxide was added to MV dye's solution as depicted in the spectrum (**C**); this could be ascribed to the oxidizing effect of hydrogen peroxide on methyl violet dye. The absorption response (**D**) of MV in the presence of hydrogen peroxide and ferrous salt solution confirms the hydroxyl radical generation in the Fenton system. The decrease in the absorption spectrum's intensity suggested that the generated hydroxyl free radicals must be reacting with methyl violet dye, the mechanism of which is already well established in the earlier reported work.¹⁴⁶ The results suggest that the •OH free radical was generated during the given experimental conditions.

The hydroxyl free radical is generated within the Fenton system following the reaction shown in **Equation 3.1**.

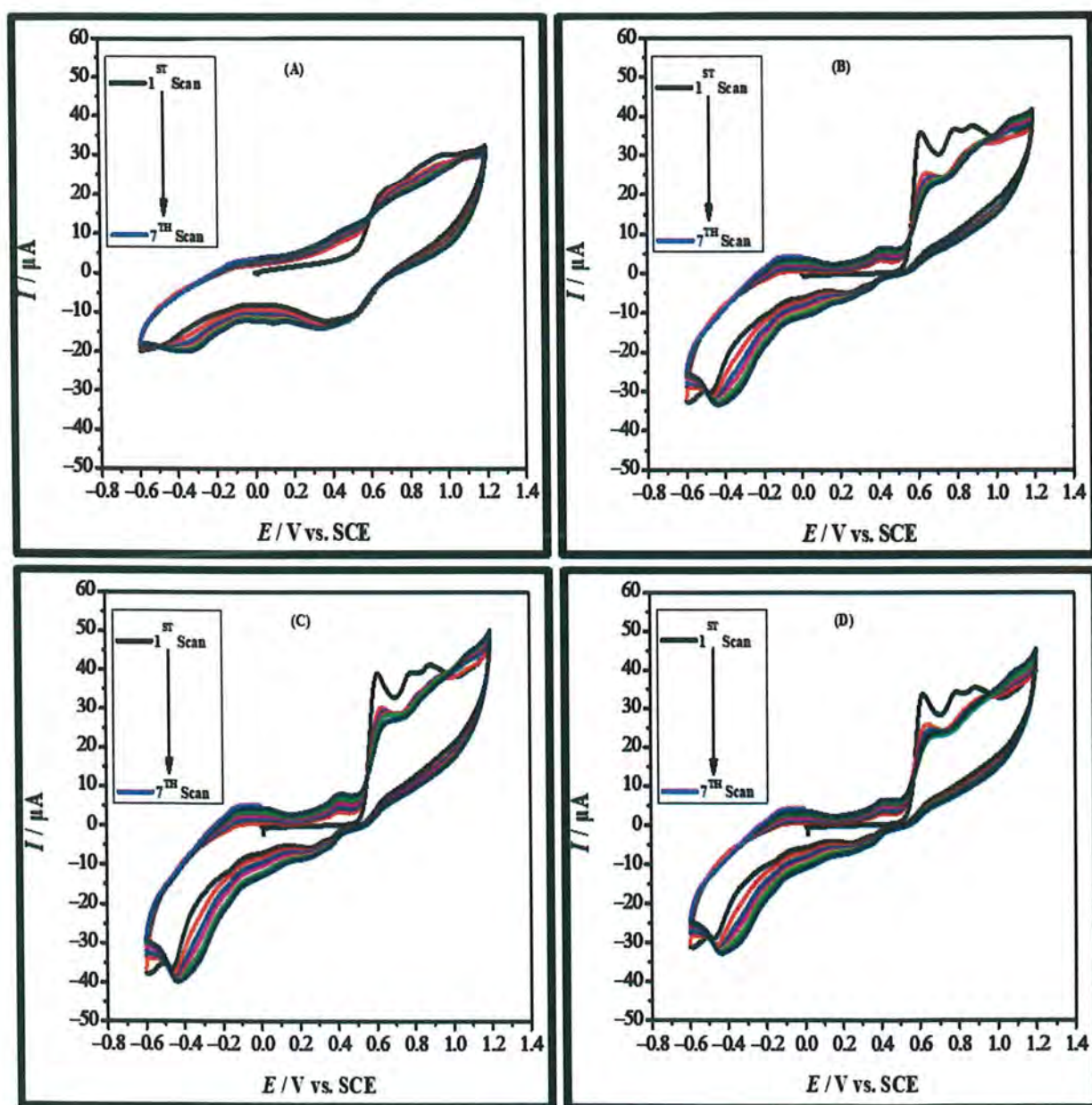


The •OH free radical generated in the above reaction possesses the capability to react with MV dye by attacking its –C=C– system, where it has a highly dense electron cloud. The reaction between •OH with MV dye has been shown in **Equation 3.2**.¹⁴⁶



3.3 Electropolymerization of o-phenylenediamine (o-PD)

The o-phenylenediamine (monomer) was electrochemically polymerized on a commercially available glassy carbon electrode (GCE) and seven (07) fabricated carbon paste electrodes (CPEs) by conducting cyclic voltammetry in the potential window ranging from -0.6 V to 1.2 V at a scan rate of 100 mV/s. The working electrodes were fabricated by following the standard procedure discussed in **Section 2.3.2.2**. Before initiating the electropolymerization experiment of o-PD, it was ensured that the surface of the electrodes was smooth and free from any impurities. The cyclic voltammograms obtained from the electropolymerization of o-phenylenediamine are shown in **Figure 3.4 (A-H)**.



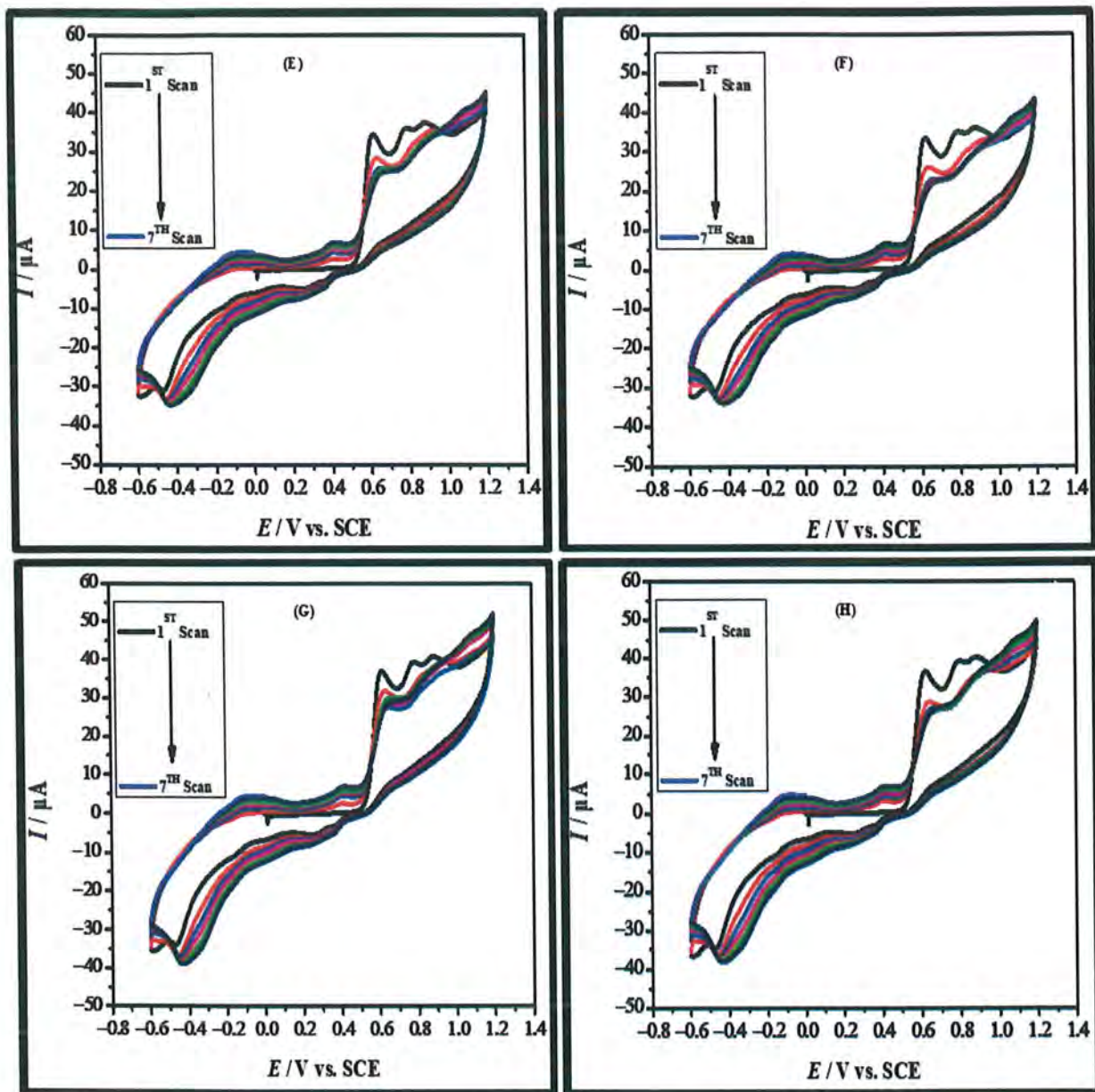


Figure 3.4 Cyclic voltammograms of electropolymerization of 0.5 mM o-PD in 0.50 M sulfuric acid on (A) GCE, (B) CPE, (C) MgO/CPE, (D) $Mg_{0.98}Zn_{0.02}O/CPE$, (E) $Mg_{0.96}Zn_{0.04}O/CPE$, (F) $Mg_{0.94}Zn_{0.06}O/CPE$, (G) $Mg_{0.92}Zn_{0.08}O/CPE$, and (H) $Mg_{0.90}Zn_{0.10}O/CPE$.

The cyclic voltammograms obtained for the electropolymerization of o-phenylenediamine on a commercially available glassy carbon electrode have been shown in **Figure 3.4 (A)**. An oxidation peak (signal) appeared at a potential of 0.674 V with a current response of 21.16 μA in the first cycle resulting in electropolymerization of o-PD. In addition to the peak appearing at 0.674 V, peaks corresponding to the reduction and oxidation peaks of poly-o-phenylenediamine (PoPD) were also observed. The voltammogram in **Figure 3.4 (A)** suggests that the response in terms of current at 0.674 V decreased continuously during

consecutive scans, and the peak potential shifted slightly towards greater potential. The decrease in the peak current with an increase in the number of cycles was attributed to the formation and slower growth of the PoPD film on the electrode's surface. When all the available electroactive sites on the electrode surface were occupied, a reproducible response in terms of current was witnessed.

The cyclic voltammograms obtained for the electrochemically induced polymerization of o-phenylenediamine on the fabricated carbon paste electrodes are shown in **Figure 3.4 (B-H)**. All the voltammograms obtained on the fabricated carbon paste electrodes exhibited a greater response in terms of current and a negative shift in oxidation potential compared to the glassy carbon electrode. The oxidation signal decreased, and the response became reproducible during successive scans; this indicated that a thin film of PoPD had saturated all the available active sites on the electrode's surface. The voltammograms suggest that the designed electrodes were preferable and more reliable for electropolymerization of o-PD than the glassy carbon electrode.

The cyclic voltammograms obtained for the fabricated electrodes are shown in **Figure 3.4 (B-H)**, indicate facile electropolymerization of o-PD, reflected from greater peak current and lower oxidation potential on MgO/CPE (**Figure 3.5 C**). An oxidation signal with a current of 40.09 μA was obtained at a potential of 0.609 V for the mentioned electrode. In contrast, the oxidation current signal obtained on the rest of the electrodes was lower and shifted to a higher oxidation potential than MgO/CPE, as shown in **Table 3.2**.

Table 3.2 Comparison of the oxidation peak current of electropolymerization of o-phenylenediamine using cyclic voltammetry on different electrodes.

S. No.	Electrode	Anodic peak current \pm 0.01 (μA)	Potential (V)
1.	Glassy Carbon Electrode (GCE)	21.16	0.674
2.	Carbon Paste Electrode (CPE)	36.08	0.613
3.	MgO/CPE	40.07	0.609
4.	$\text{Mg}_{0.98}\text{Zn}_{0.02}\text{O/CPE}$	34.49	0.618
5.	$\text{Mg}_{0.96}\text{Zn}_{0.04}\text{O/CPE}$	35.03	0.614
6.	$\text{Mg}_{0.94}\text{Zn}_{0.06}\text{O/CPE}$	34.22	0.617
7.	$\text{Mg}_{0.92}\text{Zn}_{0.08}\text{O/CPE}$	37.40	0.617
8.	$\text{Mg}_{0.90}\text{Zn}_{0.10}\text{O/CPE}$	37.68	0.617

The cyclic voltammetry results compiled in **Table 3.2** suggest that MgO/CPE was best suited for the electrochemically induced polymerization of o-phenylenediamine. The zinc-doped magnesium oxide-based carbon paste electrodes (MgZnO/CPEs) exhibited a better response in terms of polymerization current than the commercially available glassy carbon electrode, but it is evident that Zn^{2+} doping in the MgO nanomaterial did not favor the electropolymerization of o-PD to an extent to which it was favored by undoped MgO nanomaterial. The results suggested that the electrochemical oxidation of o-PD is affected by the composition of the electrode, and undoped MgO-based CPE should be selected for further investigation.

3.4 Electrochemical examination of the fabricated electrochemical probes

The voltammetric technique such as cyclic voltammetry (CV) and electrochemical impedance spectroscopy (EIS) serve as useful tools for the electrochemical characterization of the fabricated electrodes. The electrochemical techniques and their findings have been discussed in the forthcoming sections.

3.4.1 Electrochemical characterization using cyclic voltammetry

It was employed for the electrochemical characterization of the fabricated electrodes. The cyclic voltammetric behavior of CPE and MgO/CPE was investigated in a 5 mM solution of potassium hexacyanoferrate (III) (redox probe) in 0.1 M potassium chloride at a scan rate of 100 mV/s, as shown in **Figure 3.5**.

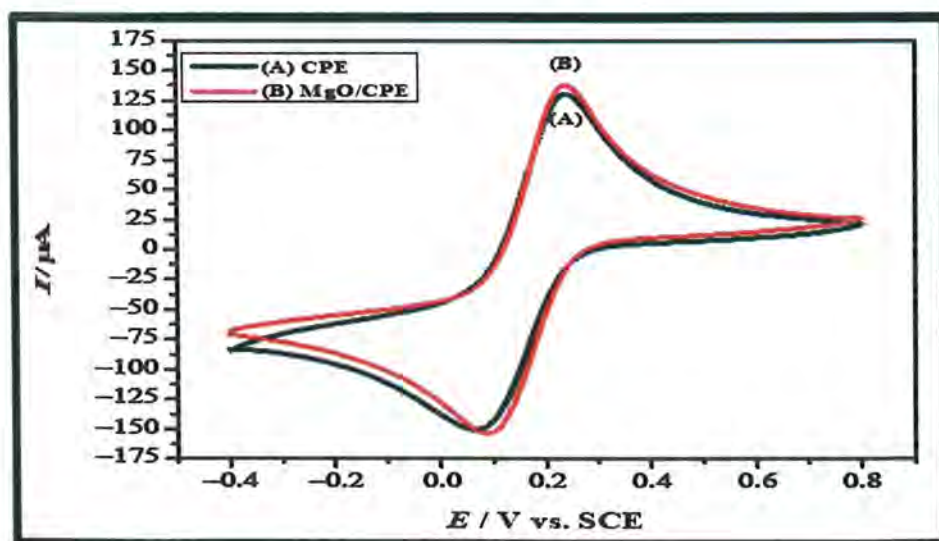


Figure 3.5 Cyclic voltammograms of (A) CPE and (B) MgO/CPE, obtained in 5mM of $K_3[Fe(CN)_6]$ (redox probe) in 0.1M KCl (supporting electrolyte) at a scan rate of 100 mV/s.

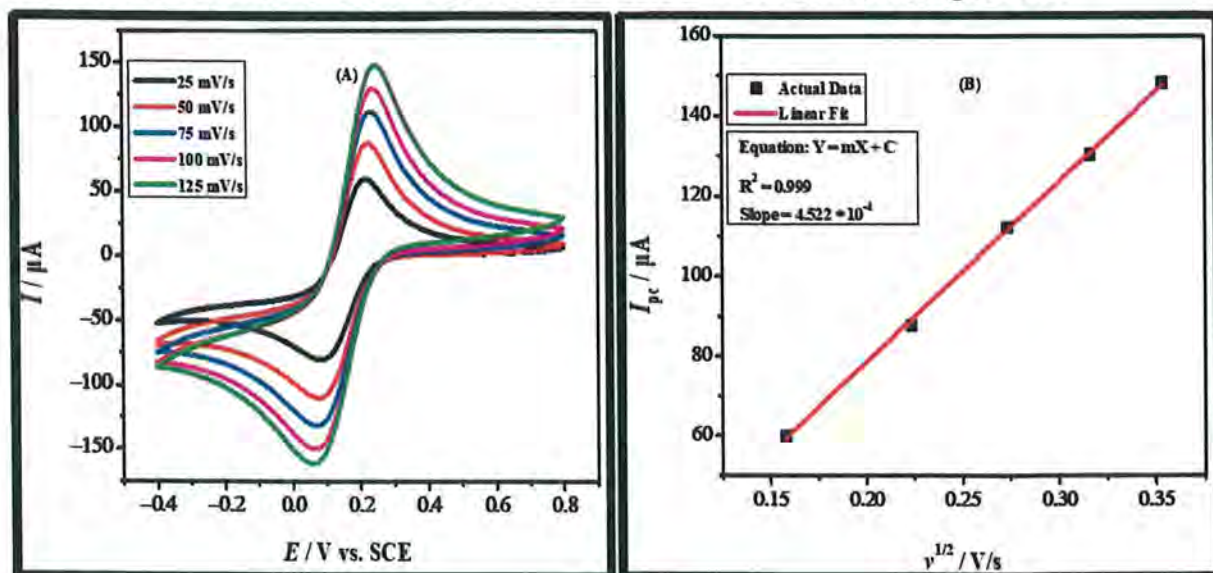
The obtained voltammograms suggested that compared to CPE, there was greater current and better reversibility exhibited on MgO/CPE, as evident from the CV data compiled in **Table 3.3**. Though there is no significant increase in the current response on MgO/CPE, it reflects that adding MgO nanomaterial is equally favorable for the fabrication of an electrochemical probing platform. Moreover, it was assessed that MgO nanomaterial induces stability and high reproducibility in the modified CPEs.

A significant factor that governs the electrochemical sensing scaffold's performance is the area of the electrode. The electro-active surface area of the electrode strongly influences the peak current response.¹⁴⁷ For investigating the change in the electro-active surface area, cyclic voltammograms were obtained in the presence of a 5 mM solution of the redox probe ($K_3[Fe(CN)_6]$) in 0.1M of the supporting electrolyte (KCl) at varied scan rates. The response in terms of current was monitored for the oxidation of Fe^{2+} to Fe^{3+} for the two differently fabricated electrodes, namely CPE and MgO/CPE. The Randles-Sevcik equation, shown in **Equation 3.4**, was used to determine the electrodes' electro-active surface area.¹⁴⁸

$$I_{pa} = 2.69 \times 10^5 n^{3/2} AD^{1/2} \nu^{1/2} C \quad (3.4)$$

Here I_{pa} represents the anodic peak current in Amperes, n is the number of electrons, D diffusion coefficient of the analyte in cm^2s^{-1} , A denotes the electro-active surface area of the electrode in cm^2 , ν symbolizes the scan rate in Vs^{-1} , and C represents the concentration of the redox probe in $mol\ cm^{-3}$. For potassium ferricyanide, $D = 7.6 \times 10^{-6}\ cm^2s^{-1}$ and $n = 1$.

Using the Randles-Sevcik equation from the slope of the graph obtained by plotting the current maxima (I_p) obtained at different scan rates vs. the square root of scan rate ($\nu^{1/2}$), the electroactive surface area of the electrodes was calculated as shown in **Figure 3.6**.



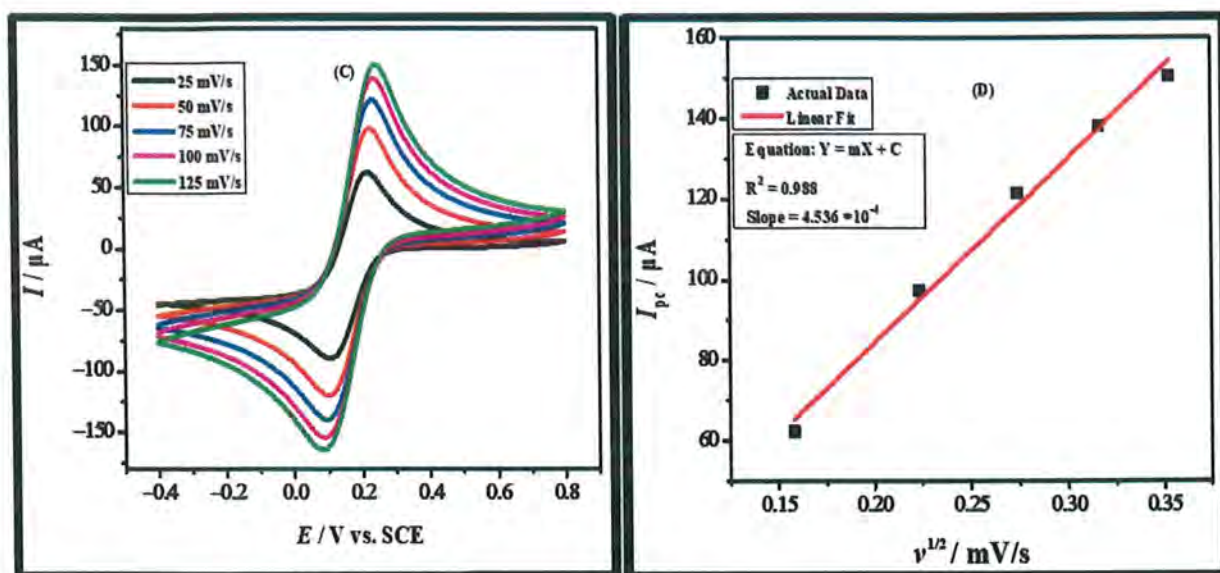


Figure 3.6 (A) Cyclic voltammograms of CPE obtained at different scan rates, (B) a plot of I_p vs. $v^{1/2}$ of CPE, (C) cyclic voltammograms of MgO/CPE obtained at different scan rates, and (D) a plot of I_p vs. $v^{1/2}$ of MgO/CPE.

The electroactive surface area of the fabricated electrodes, i.e., CPE and MgO/CPE, has been determined from the slope of the graph shown in **Figure 3.6 (B and D)**. The determined area of the electrodes has been mentioned in **Table 3.3**.

Table 3.3 Cyclic voltammetric data of CPE and MgO/CPE.

S. No.	Electrode	Electroactive Surface Area (cm^2)	Anodic peak current ± 0.01 (μA)	Peak separation (ΔE_p) (mV)
1.	CPE	0.122	130.2	174
2.	MgO/CPE	0.130	138.1	151

The findings compiled in **Table 3.3** reveal that in comparison to CPE, MgO/CPE possessed a somewhat greater electro-active surface area. The addition of MgO nanomaterial to the graphite favored the fabricated electrode by providing more binding sites for the analyte; owing to the greater surface area and more active sites on the MgO/CPE, the ease of electron transfer of the redox probe increases.

3.4.2 Electrochemical characterization using electrochemical impedance spectroscopy

It is an effective technique employed to reveal the characteristics of the interface between the electrode and the electrolytic solution. The ease of charge transferability was compared on both CPE and MgO/CPE in a 5 mM solution of potassium ferricyanide in 0.1 M potassium chloride. Nyquist plots at an amplitude of 10mV and frequencies ranging from 100 kHz to 0.1 Hz were obtained. The Nyquist plots for CPE and MgO/CPE have been represented in **Figure 3.7 (A)**. The semicircle part of the Nyquist plot represents the charge transfer resistance (R_{ct}) at the electrode-electrolyte interface. The diameter of the semicircular part serves as a measure of charge transfer resistance. In contrast, the linear part at low frequencies accounts for the diffusion-limited processes in terms of Warburg impedance (W_d).¹⁴⁹

It is evident from the Nyquist plots shown in **Figure 3.7 (A)** that the diameter of the semicircle is lower in the case of MgO/CPE than CPE, which serves as an indicator that the fabricated MgO/CPE possesses a greater number of active sites for the analyte in comparison to CPE. The MgO nanomaterial acted as a bridge between the electrode and the analyte, ultimately facilitating a faster electron transfer process.

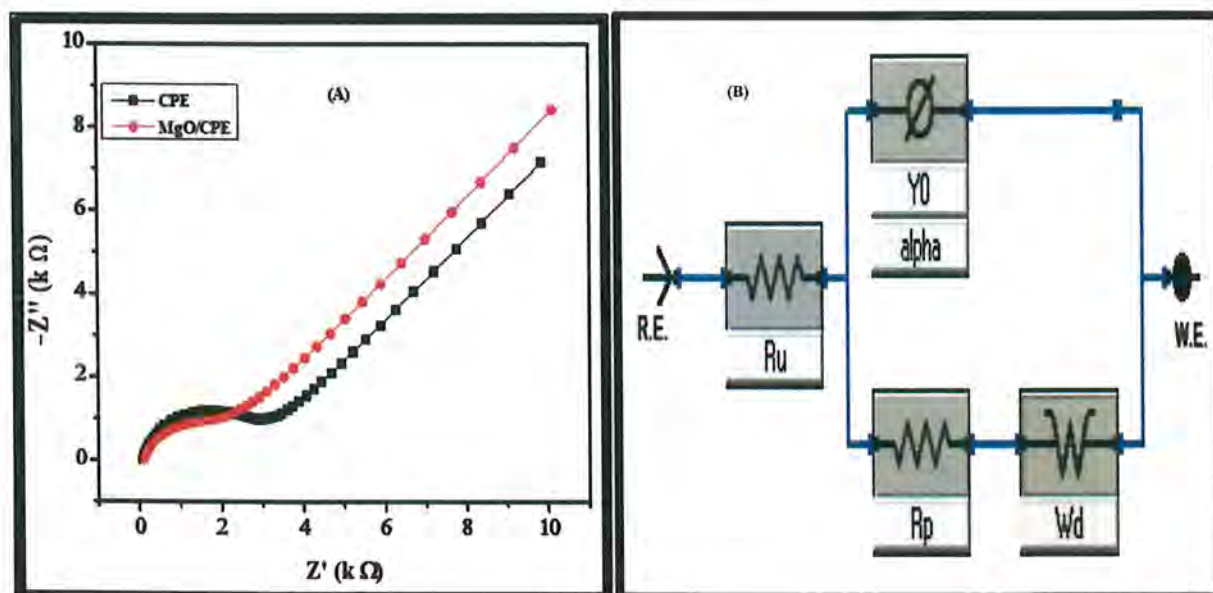


Figure 3.7 (A) Nyquist plot of CPE and MgO/CPE in a solution of 5 mM $K_3[Fe(CN)_6]$ in 0.1M KCl, and **(B)** Equivalent EIS circuit.

An equivalent circuit was fitted to the impedance spectrum obtained from EIS using Gamry Analyst version 7.05 software, shown in **Figure 3.7 (B)**. R_s (R_u) is the resistance posed by the solution, R_{ct} (R_p) is the resistance to charge transferability, C (Y_0) denotes the capacitance, and W_d represents Warburg impedance.

Table 3.4 Parameters obtained from EIS.

S. No.	Electrode	R_s (Ω)	R_{ct} ($k\Omega$)	C (μF)	W_d ($\Omega s^{1/2}$)
1.	CPE	81.4	2.730	1.081	$125 * 10^{-6}$
2.	MgO/CPE	106	1.911	3.069	$105 * 10^{-6}$

Table 3.4 suggests that in comparison to CPE, the MgO/CPE had lower R_{ct} value and exhibited a faster electron transfer kinetics due to reduced interfacial electron transfer resistance. A higher capacitance (C) value for MgO/CPE than CPE suggests that the addition of MgO nanomaterial imparted the fabricated MgO/CPE with capacitor properties. A lower value of Warburg impedance (W_d) for MgO/CPE than CPE established that diffusion mass transfer was more convenient on MgO/CPE.

3.5 Electrochemical examination of PoPD-modified electrodes

Cyclic voltammetry (CV) was employed for electropolymerization of o-PD on the fabricated electrodes. The response of PoPD-modified electrodes was then investigated using voltammetric techniques such as CV and SWV in PBS (pH=7).

3.5.1 Cyclic voltammetric examination

Cyclic voltammetry is a type of potentiodynamic electrochemical technique. Herein, the potential of the working electrode is varied linearly with time. This technique unveils the entire redox process in an electrochemical system by ramping the potential in two directions.¹⁵⁰ In addition to the faradic current, the cyclic voltammogram also contains the non-faradic current, which at times limits its applicability and interferes with the signal obtained as a result of the electron transfer (faradic) processes.

The PoPD-modified electrode was electrochemically characterized by subjecting it to cyclic voltammetry in the potential window ranging from -0.8 V to 1.2 V in 0.1 M phosphate buffer saline (PBS) (pH=7), which acted as a supporting electrolyte. The cyclic voltammogram obtained for a PoPD-modified electrode is portrayed in **Figure 3.8**.

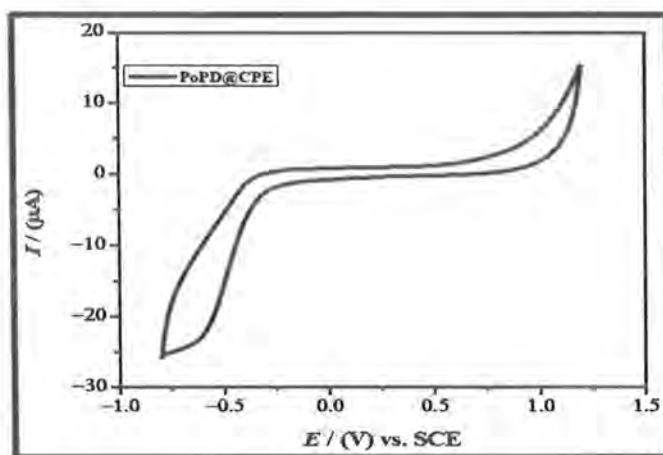


Figure 3.8 Cyclic voltammogram of PoPD-modified electrode at a scan rate of 100 mV/s.

The cyclic voltammogram depicted in **Figure 3.8** exhibits no evident response in terms of current for the polymer-modified electrode. The observation suggests that PoPD-modified electrodes should be characterized using a more sensitive technique.

3.5.2 Square wave voltammetric examination

Square wave voltammetry is also a potentiodynamic electrochemical technique. Herein, the working electrode's potential is varied in the form of small pulses.¹⁵¹ This enables it to generate a signal (faradic) that is well-resolved from the background current (non-faradic/capacitive) and imparts it with greater sensitivity than cyclic voltammetry.

The fabricated polymer-modified electrodes were characterized using square wave voltammetry by obtaining their voltammograms in the potential window ranging from 0 V to -0.8 V in 0.1 M PBS (pH=7), which acted as a supporting electrolyte. The square wave voltammogram obtained for a PoPD-modified electrode is shown in **Figure 3.9**.

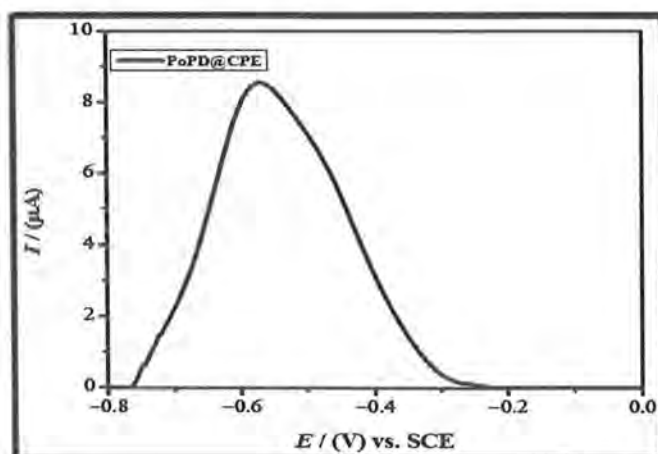


Figure 3.9 Square wave voltammogram of PoPD-modified electrode.

The square wave voltammogram in **Figure 3.9** exhibits a sharp response in terms of the current ($8.59 \mu\text{A}$) positioned at a potential of -0.572 V . The observation suggests that square wave voltammetry owing to its greater sensitivity should be employed for recording the cathodic responses of polymer-modified electrodes.

3.6 Square wave voltammetric investigation of PoPD-modified electrodes

The results of electropolymerization of o-PD on the commercially available GCE and differently fabricated CPE have been mentioned in the preceding section (**Section 3.3**). The thin film of the electropolymerized polymer (PoPD) formed on the electrode's surface serves as a shuttle to facilitate a faster electron transfer between the protein and the transducer. Once the PoPD film was formed, the next step was to examine the reduction signal of PoPD-modified electrodes in 0.1 M PBS (pH=7) using square wave voltammetry. The SWV responses of PoPD-modified GCE and fabricated CPEs have been shown in **Figure 3.10**.

The peak current depicted in **Figure 3.10 (A and B)** suggests that the reduction signal of the electropolymerized PoPD film on different electrodes existed in the range of -0.5 V to -0.6 V in 0.1 M PBS (pH=7) .

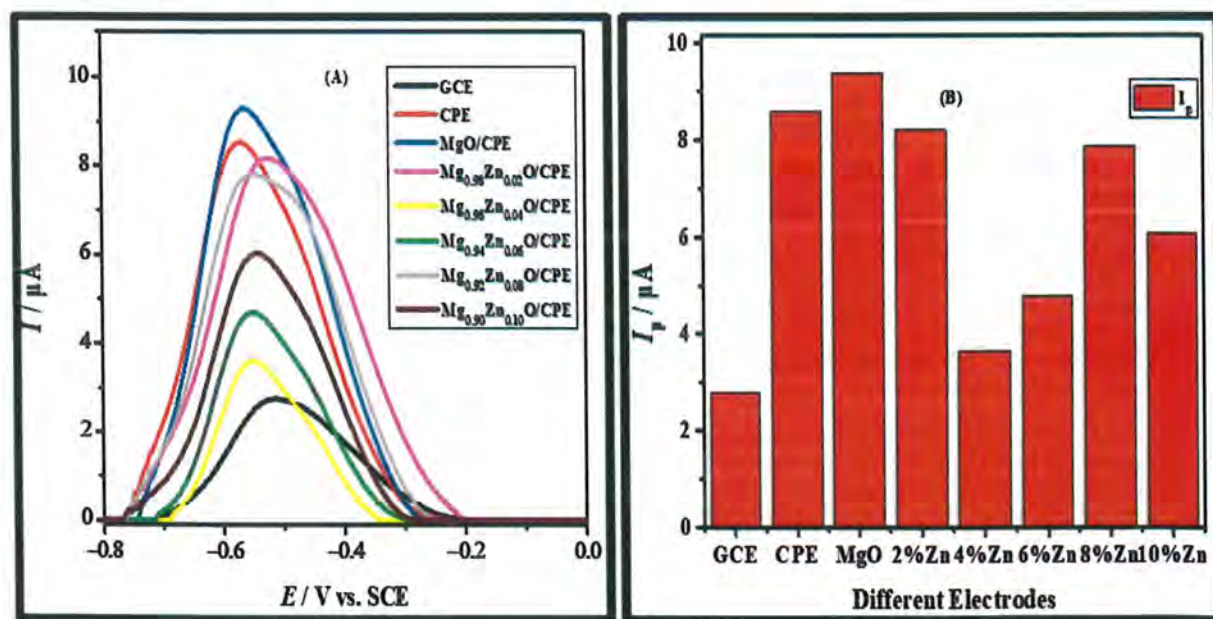


Figure 3.10 (A) Square wave voltammetric responses of polymer-modified electrodes, and (B) bar graph representing peak current responses of different electrodes.

The results obtained from SWV have been compiled in **Table 3.5**. The results suggest that all the electrodes exhibited a greater response in terms of current than the GCE; this establishes that the fabricated CPEs were preferably more suitable for designing an

electrochemical sensing platform. The PoPD-modified MgO nanomaterial-based CPE (PoPD/MgO/CPE) exhibited the greatest signal in the form of a sharp reduction peak, and the doping of Zn^{2+} in the MgO lattice resulted in a decrease in the polymer's SWV response in comparison to undoped MgO. The maximum current response obtained on PoPD-modified MgO/CPE was due to better electropolymerization and a comparatively faster electron transfer on this electrode.

Table 3.5 Square wave voltammetric response of PoPD-modified electrodes.

S. No.	Electrode	Cathodic peak current ± 0.01 (μA)	Potential (V)
1.	Glassy Carbon Electrode (GCE)	2.80	-0.528
2.	Carbon Paste Electrode (CPE)	8.58	-0.571
3.	MgO/CPE	9.39	-0.563
4.	Mg _{0.98} Zn _{0.02} O/CPE	8.21	-0.522
5.	Mg _{0.96} Zn _{0.04} O/CPE	3.65	-0.550
6.	Mg _{0.94} Zn _{0.06} O/CPE	4.78	-0.552
7.	Mg _{0.92} Zn _{0.08} O/CPE	7.87	-0.552
8.	Mg _{0.90} Zn _{0.10} O/CPE	6.07	-0.544

The SWV responses agreed with CV results, and PoPD-modified MgO-based CPE was used for further study.

3.7 Electrochemical probing of hydroxyl free radical

Electrochemical techniques such as square wave voltammetry and electrochemical impedance spectroscopy were employed to validate the designed sensing platform for the electrochemical detection of hydroxyl free radicals.

3.7.1 Square wave voltammetric investigation

Bovine serum albumin (BSA) immobilized PoPD-modified MgO/CPE was used for electrochemical sensing of hydroxyl free radical. The method for immobilizing BSA on a

polymer-modified electrode has been discussed in **Section 2.3.3.2**. A thin PoPD film on the electrode's surface facilitates a faster electron transfer. It serves as an electrochemical indicator for monitoring BSA's damage due to the hydroxyl free radical's attack.

Prior to the immobilization of the protein, the SWV response of polymer-modified MgO/CPE was recorded in 0.1 M PBS (pH=7) and is shown in **Figure 3.11 (A)**. The voltammogram **(B)** in **Figure 3.11** establishes that the BSA embedded on the PoPD-modified electrode's surface hinders the direct contact between the polymer and the solution, which results in an inhibition in the interfacial electron transfer process and decreases the current to 68% of its original value. The voltammogram **(C)** in **Figure 3.11** suggests that the current response of a protein-immobilized polymer-modified electrode decreased on exposing it to a hydroxyl free radical containing medium to a value of 27% of its original value. The SWV investigation suggests that the protein and the polymer were damaged due to the hydroxyl free radical's attack. The attenuation in PoPD's current signal suggests that the products formed post hydroxyl radical's attack resulted in a decrease in the ease of electron transfer by blocking the electrode's surface.

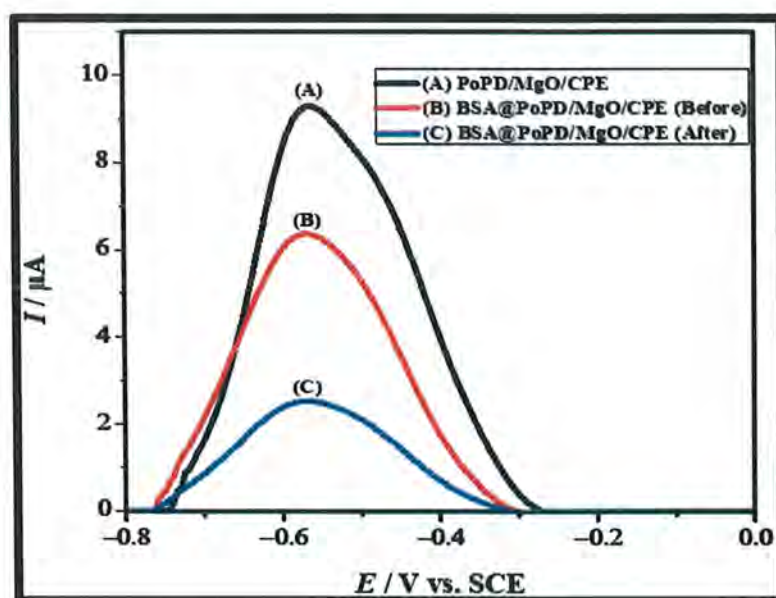


Figure 3.11 Square wave voltammograms of fabricated electrodes (A) PoPD-modified MgO/CPE, (B) BSA immobilized PoPD-modified MgO/CPE, and (C) BSA immobilized-PoPD modified MgO/CPE after hydroxyl attack.

The square wave voltammetric findings of PoPD-modified MgO/CPE and BSA immobilized PoPD-modified MgO/CPE have been summarised in **Table 3.6**.

Table 3.6 Square wave voltammetric response of protein immobilized polymer modified electrode.

S. No.	Electrode	Cathodic peak current ± 0.01 (μA)	Potential (V)
1.	PoPD/MgO/CPE	9.39	-0.563
2.	BSA@PoPD/MgO/CPE (Before)	6.39	-0.563
3.	BSA@PoPD/MgO/CPE (After)	2.56	-0.563

The results suggest that the incubation of a protein-polymer-modified electrochemical sensing platform in the Fenton system for 30 minutes with stirring at room temperature should be probed further.

3.7.1.1 Oxidative damage by hydroxyl radical

Square wave voltammetry was employed to investigate whether the embedded protein or the polymer film was more prone to free radical's attack when the designed electrochemical sensor was placed in the $\cdot\text{OH}$ -rich medium. The SWV responses have been exhibited in **Figure 3.12**.

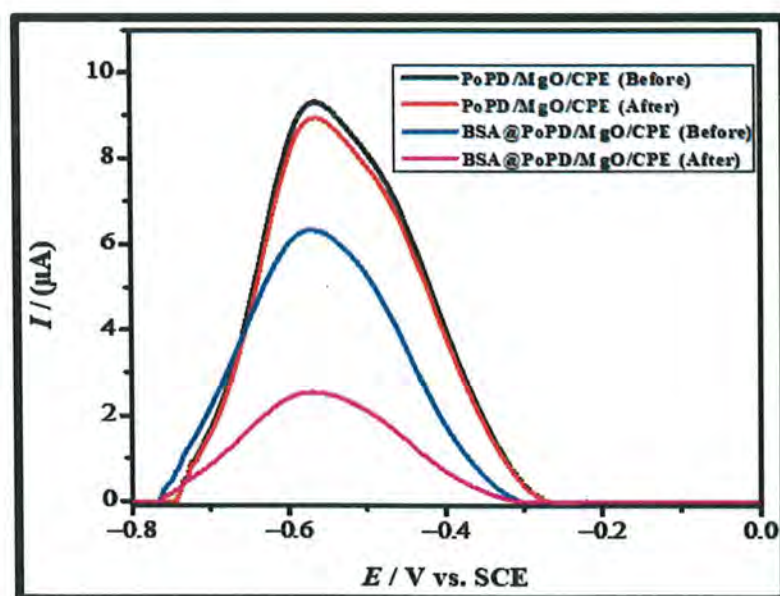


Figure 3.12 Square wave voltammograms of PoPD/MgO/CPE and BSA@PoPD/MgO/CPE in the absence and presence of hydroxyl free radical.

The voltammograms depicted in **Figure 3.12** establish that when the PoPD-modified MgO/CPE was subjected to hydroxyl attack, its current response decreased slightly, suggesting that the thin PoPD film on the electrode's surface was comparatively less affected by the presence of $\cdot\text{OH}$ in the medium. On the contrary, in the case of BSA immobilized PoPD-modified MgO/CPE, a significant loss in the current signal was observed post hydroxyl attack. The results suggest that in comparison to the polymer, the protein was more prone to hydroxyl's attack. The results compiled from the SWV study have been mentioned in **Table 3.7**.

Table 3.7 Square wave voltammetric response of polymer and protein modified electrodes pre and post hydroxyl attack.

S. No.	Electrode	Cathodic peak current ± 0.01 (μA)	Potential (V)
1.	PoPD/MgO/CPE (Before)	9.39	-0.563
2.	PoPD/MgO/CPE (After)	8.96	-0.563
3.	BSA@PoPD/MgO/CPE (Before)	6.39	-0.563
4.	BSA@PoPD/MgO/CPE (After)	2.56	-0.563

3.7.1.2 Oxidative damage of BSA in H_2O_2 , Fe^{2+} , or the Fenton system

To investigate whether the decreased current response of the fabricated electrode was due to H_2O_2 or Fe^{2+} alone or a combination of both in the Fenton system. The designed sensing scaffold was incubated individually in H_2O_2 , Fe^{2+} , and the Fenton system for 30 minutes while ensuring constant stirring. The square wave voltammetric responses were obtained in PBS (pH=7) and are exhibited in **Figure 3.13**.

The voltammograms depicted in **Figure 3.13** establish that the BSA@PoPD/MgO/CPE exhibited a similar response in the absence and presence of Fe^{2+} ; this suggested that Fe^{2+} did not contribute to the oxidative damage of the protein (BSA) immobilized at the electrode's surface. In comparison to the voltammogram obtained in the blank (PBS), the voltammogram obtained in the presence of H_2O_2 exhibited a slight decrease in the current; this establishes that the H_2O_2 oxidatively damaged BSA to a minor extent. The square wave voltammogram obtained post-incubation in the Fenton system revealed that the $\cdot\text{OH}$ free radical in the medium

attacked the BSA and PoPD immobilized on the electrode and decreased the current response significantly.

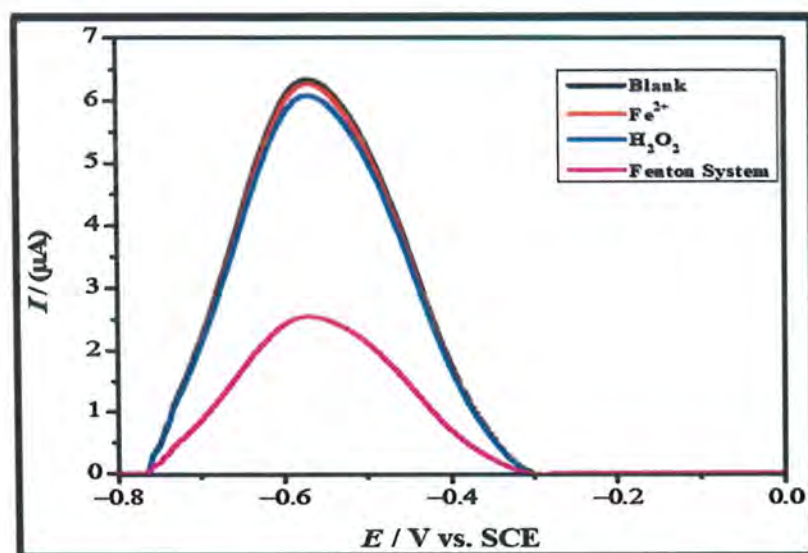


Figure 3.13 Square wave voltammograms of BSA@PoPD/MgO/CPE in the absence and presence of Fe^{2+} , H_2O_2 , or Fenton system.

The SWV findings have been compiled in **Table 3.8**, which suggests that the fabricated electrochemical sensing scaffold is sensitive and selective to a greater extent for detecting the hydroxyl free radicals.

Table 3.8 Square wave voltammetric data of BSA@PoPD/MgO/CPE

S. No.	Electrode	Cathodic peak current ± 0.01 (μA)	Potential (V)
1.	BSA@PoPD/MgO/CPE (Blank)	6.37	-0.563
2.	BSA@PoPD/MgO/CPE (Fe^{2+})	6.32	-0.563
3.	BSA@PoPD/MgO/CPE (H_2O_2)	6.10	-0.563
4.	BSA@PoPD/MgO/CPE (Fenton system)	2.56	-0.563

3.7.2 Electrochemical impedance spectroscopic investigation

EIS was employed to elucidate the nature of the interface existing between the electrode and the electrolyte, pre and post-hydroxyl free radical's attack. The ease of the charge transferability of protein immobilized PoPD-modified electrode before and after hydroxyl attack was compared to bare MgO/CPE and PoPD-modified MgO/CPE. The impedance spectra were obtained in 5 mM ($K_3[Fe(CN)_6]$) in 0.1 M KCl and are shown in **Figure 3.14**.

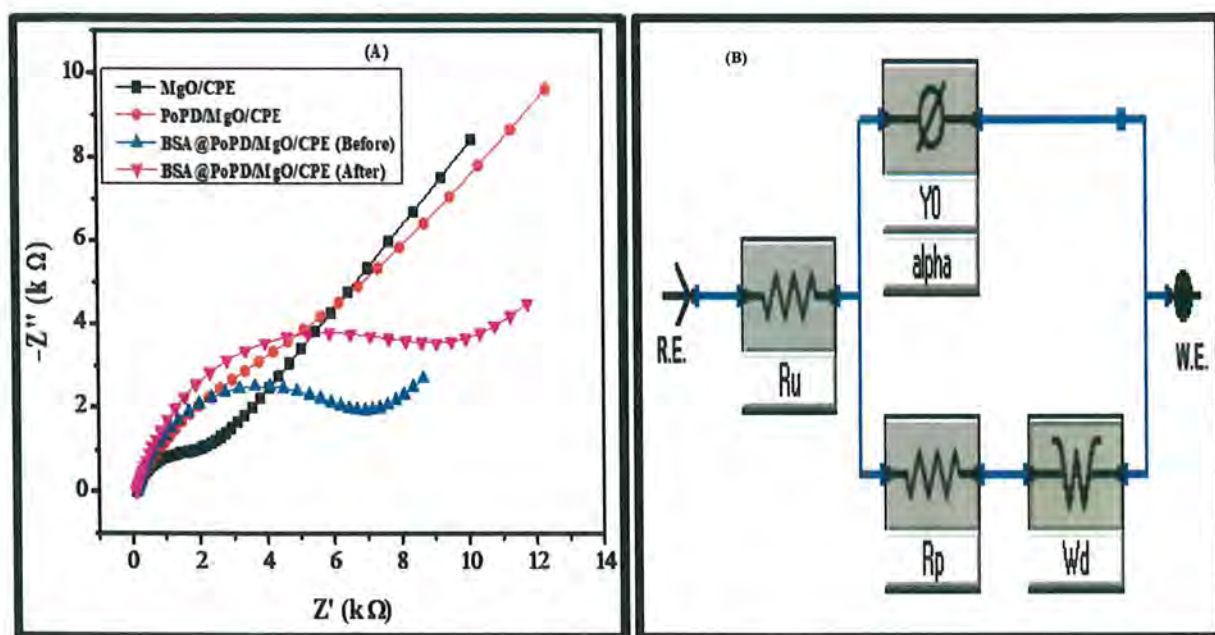


Figure 3.14 (A) Nyquist plot of BSA immobilized PoPD-modified MgO electrode and (B) Equivalent EIS circuit.

The impedance spectra in **Figure 3.14** (A) suggest that, among all the electrodes, MgO/CPE exhibited the least charge transfer resistance (R_{ct}). The electrochemical polymerization of o-PD on the electrode's surface altered the interface's features, which increased the resistance to charge transfer and imparted greater charge storing capacity (capacitance). The protein immobilization on the polymer-modified electrode blocked the electrode surface, evident from the increased R_{ct} value. The R_{ct} value of BSA immobilized PoPD-modified electrode post-hydroxyl attack increased; this establishes that the reaction of $\bullet OH$ with BSA and PoPD resulted in the denaturing of the two. An equivalent circuit shown in **Figure 3.14** (B), was fitted to the obtained EIS data using Gamry Analyst version 7.05 software. The data obtained from EIS has been compiled in **Table 3.9**.

Table 3.9 Parameters obtained from EIS.

S. No.	Electrode	R_s (Ω)	R_{ct} ($k\Omega$)	C (μF)	W_d ($\Omega s^{1/2}$)
1.	MgO/CPE	106	1.911	3.07	$105 * 10^{-6}$
2.	PoPD/MgO/CPE	148	6.126	18.4	$90.4 * 10^{-6}$
3.	BSA@ PoPD/MgO/CPE (Before)	128	6.538	8.90	$375 * 10^{-6}$
4.	BSA@ PoPD/MgO/CPE (After)	105	8.974	11.3	$240 * 10^{-6}$

CONCLUSION

Free radicals are highly reactive and short-lived chemical species capable of imparting permanent changes to the biologically essential molecules in a living system. The by-products generated from metabolic activities are classified into the reactive oxygen species (ROS) and reactive nitrogen species (RNS). ROS and RNS are essential to a certain tolerance limit, beyond which they denature biomolecules and produce highly toxic reaction intermediates. Hydroxyl radical is a type of reactive oxygen species. It is generated in a biological system by following the Fenton reaction. The exogenous and endogenous sources collectively contribute to the generation of hydroxyl radicals in a living system. The overgeneration of hydroxyl radicals leads to a biological condition known as oxidative stress, which triggers biological complexities such as cardiovascular diseases, neurodegenerative diseases, cancer, etc. The hydroxyl free radicals are directly detected by electron paramagnetic resonance spectroscopy (EPR). This technique requires a continuous supply of high concentrations of $\cdot\text{OH}$ to yield reliable results, which limits its applicability owing to the short lifetime of the hydroxyl radical. The electrochemical methods facilitate the real-time detection of hydroxyl radicals by monitoring the oxidative damage of a DNA, lipid, or protein-modified electrode. The current work proposes a protein-modified electrode for indirectly detecting the hydroxyl radical. The facile electron transfer between the immobilized protein (BSA) and the electrode was facilitated by electropolymerizing *o*-phenylenediamine (*o*-PD) on the surface of the electrode using cyclic voltammetry (CV) before anchoring the protein. The synthesized undoped and Zn^{2+} doped MgO nanomaterials were used during the electrode fabrication to investigate the most compatible nanomaterial for electropolymerization of *o*-PD. Cyclic voltammetric analysis unveiled that the undoped magnesium oxide nanomaterial was best suited for the electropolymerization of *o*-PD. Cyclic voltammetry and electrochemical impedance spectroscopy revealed that the MgO-based electrode (MgO/CPE) possessed more active sites and a lower interfacial charge transfer resistance than the bare electrode (CPE). The hydroxyl radical was generated using the Fenton reaction, and its presence was confirmed using UV-visible spectroscopy. The fabricated BSA immobilized PoPD-modified MgO-based electrochemical sensing platform was placed in the Fenton system. The electrochemical response (current) was monitored pre and post hydroxyl free radical's attack, establishing that the proposed sensor could monitor and detect hydroxyl free radicals *in vitro*.

REFERENCES

- (1) Hader, D. P.; Banaszak, A. T.; Villafane, V. E.; Narvarte, M. A.; Gonzalez, R. A.; Helbling, E. W. Anthropogenic pollution of aquatic ecosystems: emerging problems with global implications. *Sci. Total Environ.* **2020**, *713*, 136586.
- (2) Noreen, U.; Ahmed, Z.; Khalid, A.; Serafino, A. D.; Habiba, U.; Ali, F.; Hussain, M. Water pollution and occupational health hazards caused by the marble industries in district Mardan, Pakistan. *Environ. Technol. Innovation* **2019**, *16*, 100470.
- (3) Ochiai, E. *Chemicals for life and living*; Springer Berlin: Heidelberg, 2011; 3-26.
- (4) Lellis, B.; Favaro, P. C. Z.; Pamphile, J. A.; Polonio, J. C. Effects of textile dyes on health and the environment and bioremediation potential of living organisms. *Biotechnol. Res. Innovation* **2019**, *3*, 275-290.
- (5) Santo, A.; Zhu, H.; Li, Y. R. Free radicals: from health to disease. *React. Oxyg. Species* **2016**, *2*, 245-263.
- (6) Kattoor, A. J.; Pothineni, N. V. K.; Palagiri, D.; Mehta, J. L. Oxidative stress in atherosclerosis. *Curr. Atheroscler. Rep.* **2017**, *19*, 1-11.
- (7) Harris, I. S.; Denicola, G. M. The complex interplay between antioxidants and ROS in cancer. *Trends Cell Biol.* **2020**, *30*, 440-451.
- (8) Kvetkina, A.; Pisyagin, E.; Menchinskaya, E.; Yurchenko, E.; Kalina, R.; Kozlovskiy, S.; Kaluzhskiy, L.; Menshov, A.; Kim, N.; Peigneur, S. Kunitz-type peptides from sea anemones protect neuronal cells against parkinson's disease inductors via inhibition of ROS production and ATP-induced P2X7 receptor activation. *Int. J. Mol. Sci.* **2022**, *23*, 5115.
- (9) Galaup, C.; Picard, C.; Couderc, F.; Gilard, V.; Collin, F. Luminescent lanthanide complexes for reactive oxygen species biosensing and possible application in alzheimer's diseases. *FEBS J.* **2022**, *289*, 2516-2539.
- (10) Halliwell, B. Free radicals and vascular disease: how much do we know? *Br. Med. J.* **1993**, *307*, 885.
- (11) Hollan, S. Free radicals in health and disease. *Haematologia* **1995**, *26*, 177-189.
- (12) Valko, M.; Leibfritz, D.; Moncol, J.; Cronin, M. T.; Mazur, M.; Telser, J. Free radicals and antioxidants in normal physiological functions and human disease. *Int. J. Biochem. Cell Biol.* **2007**, *39*, 44-84.
- (13) Basaga, H. Biochemical aspects of free radicals. *Biochem. Cell Biol.* **1990**, *68*, 989-998.

- (14) Cheeseman, K. H.; Slater, T. F. An introduction to free radical biochemistry. *Br. Med. Bull.* **1993**, *49*, 481-493.
- (15) Fridovich, I. Reprint of: biological effects of the superoxide radical. *Arch. Biochem. Biophys.* **2022**, *726*, 109228.
- (16) Kuppusamy, P.; Zweier, J. L. Characterization of free radical generation by xanthine oxidase: evidence for hydroxyl radical generation. *J. Biol. Chem.* **1989**, *264*, 9880-9884.
- (17) Li, Y.; Liu, J.; Fu, C.; Khan, M. N.; Hu, J.; Zhao, F.; Wu, H.; Li, Z. CeO₂ nanoparticles modulate Cu-Zn superoxide dismutase and lipoxygenase-IV isozyme activities to alleviate membrane oxidative damage to improve rapeseed salt tolerance. *Environ. Sci.: Nano* **2022**, *9*, 1116-1132.
- (18) Khanaki, K.; Fekri, A.; Abedinzade, M.; Mohammadi, E.; Aghajanpour, F. Potential anti-inflammatory effect of lamium album extract through caspase-3 and cyclooxygenase-2 genes expression in a rat model of middle cerebral artery occlusion. *Folia Med.* **2022**, *64*, 275-282.
- (19) Cathcart, M. K. Regulation of superoxide anion production by NADPH oxidase in monocytes/macrophages: contributions to atherosclerosis. *Arterioscler. Thromb. Vasc. Biol.* **2004**, *24*, 23-28.
- (20) Freinbichler, W.; Bianchi, L.; Colivicchi, M. A.; Ballini, C.; Tipton, K. F.; Linert, W.; Corte, L. D. The detection of hydroxyl radicals in vivo. *J. Inorg. Biochem.* **2008**, *102*, 1329-1333.
- (21) Halliwell, B. Oxidants and human disease: Some new concepts¹. *FASEB J.* **1987**, *1*, 358-364.
- (22) Lloyd, R. V.; Hanna, P. M.; Mason, R. P. The origin of the hydroxyl radical oxygen in the fenton reaction. *Free Radical Biol. Med.* **1997**, *22*, 885-888.
- (23) Grady, J.; Chen, Y.; Chasteen, N.; Harris, D. Hydroxyl radical production during oxidative deposition of iron in ferritin. *J. Biol. Chem.* **1989**, *264*, 20224-20229.
- (24) Grey, A. D. HO₂•: the forgotten radical. *DNA Cell Biol.* **2002**, *21*, 251-257.
- (25) Cheung, E. C.; Vousden, K. H. The role of ROS in tumour development and progression. *Nat. Rev. Cancer* **2022**, *22*, 280-297.
- (26) Buettner, G. R. Superoxide dismutase in redox biology: the roles of superoxide and hydrogen peroxide. *Anti-Cancer Agents Med. Chem.* **2011**, *11*, 341-346.
- (27) Mahomoodally, M. F.; MA, L. E. R. Catalase. In *Antioxidants effects in health*; Nabavi, S. M., Silva, A., Eds.; Elsevier Netherlands: Amsterdam, 2022; pp 81-90.

- (28) Zhao, Y.; Wang, H.; Zhou, J.; Shao, Q. Glutathione peroxidase GPX1 and its dichotomous roles in cancer. *Cancers* **2022**, *14*, 2560.
- (29) Qiao, K.; Wang, C.; Huang, L.; Feng, H.; Chen, B.; Xu, M.; Su, Y.; Liu, S.; Pan, N.; Su, J. Molecular characterization of a new tetrodotoxin-binding protein, peroxiredoxin-1, from takifugu bimaculatus. *Int. J. Mol. Sci.* **2022**, *23*, 3071.
- (30) Ricciardolo, F. L.; Distefano, A.; Sabatini, F.; Folkerts, G. Reactive nitrogen species in the respiratory tract. *Eur. J. Pharmacol.* **2006**, *533*, 240-252.
- (31) Arias, F.; Franco, M. F.; Romero, M.; Duarte, J.; Carrion, M. D.; Camacho, M. E. Bioactive imidamide-based compounds targeted against nitric oxide synthase. *Bioorg. Chem.* **2022**, *120*, 105637.
- (32) Subczynski, W. K.; Lomnicka, M.; Hyde, J. S. Permeability of nitric oxide through lipid bilayer membranes. *Free Radical Res.* **1996**, *24*, 343-349.
- (33) Wink, D. A.; Mitchell, J. B. Chemical biology of nitric oxide: insights into regulatory, cytotoxic, and cytoprotective mechanisms of nitric oxide. *Free Radical Biol. Med.* **1998**, *25*, 434-456.
- (34) Stamler, J. S. Redox signaling: nitrosylation and related target interactions of nitric oxide. *Cell* **1994**, *78*, 931-936.
- (35) Epe, B.; Ballmaier, D.; Roussyn, I.; Briviba, K.; Sies, H. DNA damage by peroxynitrite characterized with DNA repair enzymes. *Nucleic Acids Res.* **1996**, *24*, 4105-4110.
- (36) Martemucci, G.; Costagliola, C.; Mariano, M.; D'andrea, L.; Napolitano, P.; D'Alessandro, A. G. Free radical properties, source and targets, antioxidant consumption and health. *Oxygen* **2022**, *2*, 48-78.
- (37) Raha, S.; Robinson, B. H. Mitochondria, oxygen free radicals, disease and ageing. *Trends Biochem. Sci.* **2000**, *25*, 502-508.
- (38) Figueira, T. R.; Barros, M. H.; Camargo, A. A.; Castilho, R. F.; Ferreira, J. C.; Kowaltowski, A. J.; Sluse, F. E.; Souza, P. N. C.; Vercesi, A. E. Mitochondria as a source of reactive oxygen and nitrogen species: from molecular mechanisms to human health. *Antioxid. Redox Signal.* **2013**, *18*, 2029-2074.
- (39) Neve, E.; Ingelman, S. M. Cytochrome P450 proteins: retention and distribution from the endoplasmic reticulum. *Curr. Opin. Drug Discovery Dev.* **2010**, *13*, 78-85.
- (40) Lu, Y.; Wang, R.; Sun, Y.; Tian, M.; Dong, B. Endoplasmic reticulum-specific fluorescent probe for the two-photon imaging of endogenous superoxide anion ($O_2^{\bullet-}$) in live cells and zebrafishes. *Talanta* **2021**, *225*, 122020.

- (41) Perichon, R.; Bourre, J.; Kelly, J.; Roth, G. The role of peroxisomes in aging. *Cell. Mol. Life Sci.* **1998**, *54*, 641-652.
- (42) Bafana, A.; Dutt, S.; Kumar, S.; Ahuja, P. S. Superoxide dismutase: an industrial perspective. *Crit. Rev. Biotechnol.* **2011**, *31*, 65-76.
- (43) Liu, M.; Yang, C.; Chu, Q.; Fu, X.; Zhang, Y.; Sun, G. Superoxide dismutase and glutathione reductase as indicators of oxidative stress levels may relate to geriatric hip fractures' survival and walking ability: a propensity score matching study. *Clin. Interv. Aging* **2022**, *17*, 1081.
- (44) Flohe, L.; Toppo, S.; Orian, L. The glutathione peroxidase family: discoveries and mechanism. *Free Radic. Biol. Med.* **2022**, *187*, 113-122.
- (45) Ali, F.; Manzoor, U.; Bhattacharya, R.; Bansal, A. K.; Chandrashekharaiyah, K. S.; Singh, L. R.; Saraswati, S. M.; Uversky, V.; Dar, T. A. Brain metabolite, myo-inositol, inhibits catalase activity: a mechanism of the distortion of the antioxidant defense system in alzheimer's disease. *ACS Omega* **2022**, *7*, 12690-12700.
- (46) Arribas, S. M.; Martin, C. M. A. Antioxidant foods and cardiometabolic health. *Antioxidants* **2022**, *11*, 746.
- (47) Hajam, Y. A.; Rani, R.; Ganie, S. Y.; Sheikh, T. A.; Javaid, D.; Qadri, S. S.; Pramodh, S.; Alsulimani, A.; Alkhanani, M. F.; Harakeh, S. Oxidative stress in human pathology and aging: molecular mechanisms and perspectives. *Cells* **2022**, *11*, 552.
- (48) Spector, A. Oxidative stress and disease. *J. Ocul. Pharmacol. Ther.* **2000**, *16*, 193-201.
- (49) Oberley, L. W. Free radicals and diabetes. *Free Radical Biol. Med.* **1988**, *5*, 113-124.
- (50) Taghavi, F.; Moosavi, M. A. A. Free radicals, diabetes, and its complexities. In *Plant and human health*; Ozturk, M., Hakeem, K. R., Eds.; Springer Denmark: Cham, 2019; pp 1-41.
- (51) Hassan, W.; Noreen, H.; Rehman, S.; Kamal, M. A.; Darocha, J. B. Association of oxidative stress with neurological disorders. *Curr. Neuropharmacol.* **2022**, *20*, 1046-1072.
- (52) Rummel, N. G.; Butterfield, D. A. Altered metabolism in alzheimer disease brain: role of oxidative stress. *Antioxid. Redox Signaling* **2022**, *36*, 1289-1305.
- (53) Blesa, J.; Damas, I. T.; Varela, A. Q.; Jackson, L. V. R. Oxidative stress and parkinson's disease. *Front. Neuroanat.* **2015**, *9*, 91.
- (54) Xiong, L.; McCoy, M.; Komuro, H.; West, X. Z.; Yakubenko, V.; Gao, D.; Dudiki, T.; Milo, A.; Chen, J.; Podrez, E. A. Inflammation-dependent oxidative stress metabolites

- as a hallmark of amyotrophic lateral sclerosis. *Free Radical Biol. Med.* **2022**, *178*, 125-133.
- (55) Renaudin, X. Reactive oxygen species and DNA damage response in cancer. *Int. Rev. Cell Mol. Biol.* **2021**, *364*, 139-161.
- (56) Alvarez, G. R. Free radicals, oxidative stress, and DNA metabolism in human cancer. *Cancer Invest.* **1999**, *17*, 376-377.
- (57) Walling, C. Fenton's reagent revisited. *Acc. Chem. Res.* **1975**, *8*, 125-131.
- (58) Kehrer, J. P. The haber–weiss reaction and mechanisms of toxicity. *Toxicology* **2000**, *149*, 43-50.
- (59) Fan, H. J.; Huang, S. T.; Chung, W. H.; Jan, J. L.; Lin, W. Y.; Chen, C. C. Degradation pathways of crystal violet by fenton and fenton-like systems: condition optimization and intermediate separation and identification. *J. Hazard. Mater.* **2009**, *171*, 1032-1044.
- (60) Brillas, E.; Sires, I.; Oturan, M. A. Electro-fenton process and related electrochemical technologies based on fenton's reaction chemistry. *Chem. Rev.* **2009**, *109*, 6570-6631.
- (61) Bremner, D. H.; Burgess, A. E.; Li, F. B. Coupling of chemical, electrochemical and ultrasonic energies for controlled generation of hydroxyl radicals: direct synthesis of phenol by benzene hydroxylation. *Appl. Catal., A* **2000**, *203*, 111-120.
- (62) Medien, H. A.; Khalil, S. M. Kinetics of the oxidative decolorization of some organic dyes utilizing fenton-like reaction in water. *J. King Saud Univ. Sci.* **2010**, *22*, 147-153.
- (63) Wang, Y.; Xiong, H.; Zhang, X.; Wang, S. Electrochemical biosensors for the detection of oxidative DNA damage induced by fenton reagents in ionic liquid. *Sens. Actuators, B* **2012**, *161*, 274-278.
- (64) Floyd, R. A.; Watson, J. J.; Wong, P. K.; Altmiller, D. H.; Rickard, R. C. Hydroxyl free radical adduct of deoxyguanosine: sensitive detection and mechanisms of formation. *Free Rad. Res. Commun.* **1986**, *1*, 163-172.
- (65) Cadet, J.; Delatour, T.; Douki, T.; Gasparutto, D.; Pouget, J. P.; Ravanat, J. L.; Sauvaigo, S. Hydroxyl radicals and DNA base damage. *Mutat. Res.-Fundam. Mol. Mech. Mutagen.* **1999**, *424*, 9-21.
- (66) Phaniendra, A.; Jestadi, D. B.; Periyasamy, L. Free radicals: properties, sources, targets, and their implication in various diseases. *Indian J. Clin. Biochem.* **2015**, *30*, 11-26.
- (67) Vileno, B.; Port, L. Y.; Gimenez, A. E. Electron paramagnetic resonance and spin trapping to detect free radicals from allergenic hydroperoxides in contact with the skin: from the molecule to the tissue. *Contact Derm.* **2022**, *86*, 241-253.

- (68) Duanghathaipornsuk, S.; Kanel, S.; Haushalter, E. F.; Ruetz, J. E.; Kim, D. S. Detection of hydroxyl radicals using cerium oxide/graphene oxide composite on prussian blue. *Nanomaterials* **2020**, *10*, 1136.
- (69) Bergh, V. V.; Vanhees, I.; Boer, R. D.; Compennolle, F.; Vinckier, C. Identification of the oxidation products of the reaction between α -pinene and hydroxyl radicals by gas and high-performance liquid chromatography with mass spectrometric detection. *J. Chromatogr. A* **2000**, *896*, 135-148.
- (70) Michail, K.; Siraki, A. G. Post-trapping derivatization of radical-derived EPR-silent adducts: application to free radical detection by HPLC/UV in chemical, biochemical, and biological systems and comparison with EPR spectroscopy. *Anal. Chem.* **2012**, *84*, 6739-6746.
- (71) Lei, K.; Sun, M.; Du, L.; Zhang, X.; Yu, H.; Wang, S.; Hayat, T.; Alsaedi, A. Sensitive determination of endogenous hydroxyl radical in live cell by a BODIPY based fluorescent probe. *Talanta* **2017**, *170*, 314-321.
- (72) Huang, Y.; Sinha, A.; Zhao, H.; Dang, X.; Zhang, Y.; Quan, X. Real time detection of hazardous hydroxyl radical using an electrochemical approach. *ChemistrySelect* **2019**, *4*, 12507-12511.
- (73) Catapano, M. C.; Protti, M.; Fontana, T.; Mandrioli, R.; Mladenka, P.; Micolini, L. An original HPLC method with coulometric detection to monitor hydroxyl radical generation via fenton chemistry. *Molecules* **2019**, *24*, 3066.
- (74) Scholz, F.; Gonzalez, G. L.; Carvalho, L. M.; Hilgemann, M.; Brainina, K. Z.; Kahlert, H.; Jack, R. S.; Minh, D. T. Indirect electrochemical sensing of radicals and radical scavengers in biological matrices. *Angew. Chem. Int. Ed.* **2007**, *46*, 8079-8081.
- (75) Guo, Q.; Yue, Q.; Zhao, J.; Wang, L.; Wang, H.; Wei, X.; Liu, J.; Jia, J. How far can hydroxyl radicals travel? An electrochemical study based on a DNA mediated electron transfer process. *Chem. Commun.* **2011**, *47*, 11906-11908.
- (76) Barroso, M. F.; Luna, M. A.; Moyano, F.; Delerue, M. C.; Correa, N. M.; Molina, P. G. Study of lipid peroxidation and ascorbic acid protective role in large unilamellar vesicles from a new electrochemical performance. *Bioelectrochemistry* **2018**, *120*, 120-126.
- (77) Wang, Y.; Xiong, H.; Zhang, X.; Gu, H.; Wang, S. An electrochemical biosensor for rapid detection of bovine serum albumin damage induced by hydroxyl radicals in room temperature ionic liquid. *Sens. Actuators, B* **2013**, *188*, 741-746.

- (78) Hulanicki, A.; Glab, S.; Ingman, F. Chemical sensors: definitions and classification. *Pure Appl. Chem.* **1991**, *63*, 1247-1250.
- (79) Wang, P.; Liu, Q. Basics of sensors and measurement. In *Biomedical sensors and measurement*; Springer Berlin: Heidelberg, 2011; pp 17-50.
- (80) Rodriguez, M. S.; Alda, M. J.; Barcelo, D. Biosensors as useful tools for environmental analysis and monitoring. *Anal. Bioanal. Chem.* **2006**, *386*, 1025-1041.
- (81) Luong, J.; Mulchandani, A.; Guilbault, G. Developments and applications of biosensors. *Trends Biotechnol.* **1988**, *6*, 310-316.
- (82) Peura, R. A.; Kun, S. Physical sensors. In *Handbook of chemical and biological sensors*; Taylor, R. F., Schultz, J. S., Eds.; CRC Press Florida: Boca Raton, 1996; pp 11-44.
- (83) Li, S.; Zhang, Y.; Wang, Y.; Xia, K.; Yin, Z.; Wang, H.; Zhang, M.; Liang, X.; Lu, H.; Zhu, M. Physical sensors for skin-inspired electronics. *InfoMat* **2020**, *2*, 184-211.
- (84) Marcellis, A. D.; Ferri, G. Physical and chemical sensors. In *Analog circuits and systems for voltage-mode and current-mode sensor interfacing applications*; Springer Netherlands: Dordrecht, 2011; pp 1-35.
- (85) Huang, X. J.; Choi, Y. K. Chemical sensors based on nanostructured materials. *Sens. Actuators, B* **2007**, *122*, 659-671.
- (86) Schroeder, V.; Savagatrup, S.; He, M.; Lin, S.; Swager, T. M. Carbon nanotube chemical sensors. *Chem. Rev.* **2018**, *119*, 599-663.
- (87) Elsherif, M.; Salih, A. E.; Munoz, M. G.; Alam, F.; Alqattan, B.; Antonysamy, D. S.; Zaki, M. F.; Yetisen, A. K.; Park, S.; Wilkinson, T. D. Optical fiber sensors: working principle, applications, and limitations. *Adv. Photonics Res.* **2022**, *3*, 2100371.
- (88) McDonagh, C.; Burke, C. S.; MacCraith, B. D. Optical chemical sensors. *Chem. Rev.* **2008**, *108*, 400-422.
- (89) Lieberzeit, P. A.; Afzal, A.; Rehman, A.; Dickert, F. L. Nanoparticles for detecting pollutants and degradation processes with mass-sensitive sensors. *Sens. Actuators, B* **2007**, *127*, 132-136.
- (90) Abdollahi, A.; Jiang, Z.; Arabshahi, S. A. Evaluation on mass sensitivity of SAW sensors for different piezoelectric materials using finite-element analysis. *IEEE Trans. Ultrason. Ferroelectr. Freq. Control* **2007**, *54*, 2446-2455.
- (91) Bakker, E.; Telting, D. M. Electrochemical sensors. *Anal. Chem.* **2002**, *74*, 2781-2800.
- (92) Privett, B. J.; Shin, J. H.; Schoenfisch, M. H. Electrochemical sensors. *Anal. Chem.* **2008**, *80*, 4499-4517.

- (93) Bian, C.; Xiong, H.; Zhang, X.; Ye, Y.; Gu, H.; Wang, S. Electrochemical detection of BSA damage induced by Fenton reagents in room temperature ionic liquid. *Sens. Actuators, B* **2012**, *169*, 368-373.
- (94) Wang, Y.; Xiong, H.; Zhang, X.; Wang, S. Electrochemical study of bovine serum albumin damage induced by fenton reaction using tris (2, 2'-bipyridyl) cobalt (III) perchlorate as the electroactive indicator. *Electrochim. Acta* **2012**, *67*, 147-151.
- (95) Noll, T.; Noll, G. Strategies for "wiring" redox-active proteins to electrodes and applications in biosensors, biofuel cells, and nanotechnology. *Chem. Soc. Rev.* **2011**, *40*, 3564-3576.
- (96) Umana, M.; Waller, J. Protein-modified electrodes. The glucose oxidase/polypyrrole system. *Anal. Chem.* **1986**, *58*, 2979-2983.
- (97) Feng, L. J.; Zhang, X. H.; Zhao, D. M.; Wang, S. F. Electrochemical studies of bovine serum albumin immobilization onto the poly-o-phenylenediamine and carbon-coated nickel composite film and its interaction with papaverine. *Sens. Actuators, B* **2011**, *152*, 88-93.
- (98) Kuwahara, T.; Ohta, H.; Kondo, M.; Shimomura, M. Immobilization of glucose oxidase on carbon paper electrodes modified with conducting polymer and its application to a glucose fuel cell. *Bioelectrochemistry* **2008**, *74*, 66-72.
- (99) Pandey, P.; Prakash, R. Characterization of electropolymerized polyindole: application in the construction of a solid-state, ion-selective electrode. *J. Electrochem. Soc.* **1998**, *145*, 4103.
- (100) Parente, A.; Marques, E.; Azevedo, W.; Diniz, F.; Melo, E. Glucose biosensor using glucose oxidase immobilized in polyaniline. *Appl. Biochem. Biotechnol.* **1992**, *37*, 267-273.
- (101) Yagati, A. K.; Choi, J. W. Protein based electrochemical biosensors for H₂O₂ detection towards clinical diagnostics. *Electroanalysis* **2014**, *26*, 1259-1276.
- (102) Bianco, P. Protein modified and membrane electrodes: strategies for the development of biomolecular sensors. *Rev. Mol. Biotechnol.* **2002**, *82*, 393-409.
- (103) Mechler, A.; Nawaratna, G.; Aguilar, M. I.; Martin, L. L. A study of protein electrochemistry on a supported membrane electrode. *Int. J. Pept. Res. Ther.* **2006**, *12*, 217-224.
- (104) Multhauf, R. P. A history of magnesia alba. *Ann. Sci.* **1976**, *33*, 197-200.
- (105) Hornak, J. Synthesis, properties, and selected technical applications of magnesium oxide nanoparticles: a review. *Int. J. Mol. Sci.* **2021**, *22*, 12752.

- (106) Feynman, R. P. Plenty of room at the bottom. In *APS annual meeting*, 1959.
- (107) Biswas, P.; Wu, C. Y. Nanoparticles and the environment. *J. Air Waste Manag. Assoc.* **2005**, *55*, 708-746.
- (108) Manzoor, U.; Islam, M.; Tabassam, L.; Rahman, S. U. Quantum confinement effect in ZnO nanoparticles synthesized by co-precipitate method. *Physica E* **2009**, *41*, 1669-1672.
- (109) Begum, N.; Bhatti, A.; Jabeen, F.; Rubini, S.; Martelli, F. Phonon confinement effect in III-V nanowires. In *Nanowires*; Prete, P., Ed.; IntechOpen: London, 2010; pp 255-272.
- (110) Baxter, J. B.; Schmuttenmaer, C. A. Conductivity of ZnO nanowires, nanoparticles, and thin films using time-resolved terahertz spectroscopy. *J. Phys. Chem. B* **2006**, *110*, 25229-25239.
- (111) Ko, S. P.; Soh, J. Y.; Kim, Y. K. Control of magnetic behavior in Fe₃O₄ nanostructures. *IEEE Trans. Magn.* **2005**, *41*, 3304-3306.
- (112) Choudhari, K. S.; Choi, C. H.; Chidangil, S.; George, S. D. Recent progress in the fabrication and optical properties of nanoporous anodic alumina. *Nanomaterials* **2022**, *12*, 444.
- (113) Yan, Y.; King, S. C.; Li, M.; Galy, T.; Marszewski, M.; Kang, J. S.; Pilon, L.; Hu, Y.; Tolbert, S. H. Exploring the effect of porous structure on thermal conductivity in templated mesoporous silica films. *J. Phys. Chem. C* **2019**, *123*, 21721-21730.
- (114) Singh, J. P.; Won, S. O.; Lim, W. C.; Shim, C. H.; Chae, K. H. Optical behavior of MgO nanoparticles investigated using diffuse reflectance and near edge X-ray absorption spectroscopy. *Mater. Lett.* **2017**, *198*, 34-37.
- (115) Yin, D.; Chen, C.; Saito, M.; Inoue, K.; Ikuhara, Y. Ceramic phases with one-dimensional long-range order. *Nat. Mater.* **2019**, *18*, 19-23.
- (116) Liu, J.; Wang, W.; Guo, Z.; Zeng, R.; Dou, S.; Chen, X. Peashell-like nanostructure—a new kind of one-dimensional nanostructure: the case of magnesium oxide. *Chem. Commun.* **2010**, *46*, 3887-3889.
- (117) Singh, J. P.; Singh, V.; Sharma, A.; Pandey, G.; Chae, K. H.; Lee, S. Approaches to synthesize MgO nanostructures for diverse applications. *Heliyon* **2020**, *6*, e04882.
- (118) Zheng, W.; Dong, Y.; Li, T.; Chen, J.; Chen, X.; Dai, Y.; He, G. MgO blocking layer induced highly UV responsive TiO₂ nanoparticles based self-powered photodetectors. *J. Alloys Compd.* **2021**, *869*, 159299.

- (119) Yadav, L. R.; Lingaraju, K.; Manjunath, K.; Raghu, G.; Kumar, K. S.; Nagaraju, G. Synergistic effect of MgO nanoparticles for electrochemical sensing, photocatalytic-dye degradation and antibacterial activity. *Mater. Res. Express* **2017**, *4*, 025028.
- (120) Mahdavi, S.; Jalali, M.; Afkhami, A. Heavy metals removal from aqueous solutions using TiO₂, MgO, and Al₂O₃ nanoparticles. *Chem. Eng. Commun.* **2013**, *200*, 448-470.
- (121) Stolzenburg, P.; Capdevielle, A.; Teychene, S.; Biscans, B. Struvite precipitation with MgO as a precursor: application to wastewater treatment. *Chem. Eng. Sci.* **2015**, *133*, 9-15.
- (122) Rao, C. N.; Nakate, U. T.; Choudhary, R.; Kale, S. Defect-induced magneto-optic properties of MgO nanoparticles realized as optical-fiber-based low-field magnetic sensor. *Appl. Phys. Lett.* **2013**, *103*, 151107.
- (123) Han, E.; Li, Y.; Zhu, L.; Zhao, L. The effect of MgO coating on Li_{1.17}Mn_{0.48}Ni_{0.23}Co_{0.12}O₂ cathode material for lithium ion batteries. *Solid State Ionics* **2014**, *255*, 113-119.
- (124) Song, Z.; Xu, H. Splitting methanol on ultra-thin MgO (100) films deposited on a Mo substrate. *Phys. Chem. Chem. Phys.* **2017**, *19*, 7245-7251.
- (125) Behnam, R.; Morshed, M.; Tavanai, H.; Ghiaci, M. Destructive adsorption of diazinon pesticide by activated carbon nanofibers containing Al₂O₃ and MgO nanoparticles. *Bull. Environ. Contam. Toxicol.* **2013**, *91*, 475-480.
- (126) Slivka, A.; Cohen, G. Hydroxyl radical attack on dopamine. *J. Biol. Chem.* **1985**, *260*, 15466-15472.
- (127) Feix, J. B.; Kalyanaraman, B. Production of singlet oxygen-derived hydroxyl radical adducts during merocyanine-540-mediated photosensitization: analysis by ESR-spin trapping and HPLC with electrochemical detection. *Arch. Biochem. Biophys.* **1991**, *291*, 43-51.
- (128) Stemarie, L.; Boismenu, D.; Vachon, L.; Montgomery, J. Evaluation of sodium 4-hydroxybenzoate as an hydroxyl radical trap using gas chromatography–mass spectrometry and high-performance liquid chromatography with electrochemical detection. *Anal. Biochem.* **1996**, *241*, 67-74.
- (129) Kato, D.; Komoriya, M.; Nakamoto, K.; Kurita, R.; Hirono, S.; Niwa, O. Electrochemical determination of oxidative damaged DNA with high sensitivity and stability using a nanocarbon film. *Anal. Sci.* **2011**, *27*, 703.

- (130) Bian, C.; Xiong, H.; Zhang, X.; Wen, W.; Wang, S. An electrochemical biosensor for analysis of fenton-mediated oxidative damage to BSA using poly-o-phenylenediamine as electroactive probe. *Biosens. Bioelectron.* **2011**, *28*, 216-220.
- (131) Jabeen, E.; Janjua, N. K.; Ahmed, S.; Dominguez, A. E.; Jacob, C. A selective and sensitive monitoring of the OH radical using flavonoid-modified electrodes. *Electrochim. Acta* **2017**, *258*, 228-235.
- (132) Wang, T. T.; Huang, Z. L.; Xu, Q.; Hu, X. Y. Simple and sensitive determination of hydroxyl radical in atmosphere based on an electrochemically activated glassy carbon electrode. *Int. J. Environ. Anal. Chem.* **2018**, *98*, 477-491.
- (133) Duanghathaipornsuk, S.; Kim, D. S.; Phares, T. L.; Li, C. H.; Jinschek, J. R.; Alba, R. A. C. Supersensitive CeO_x-based nanocomposite sensor for the electrochemical detection of hydroxyl free radicals. *Nanoscale* **2021**, *13*, 5136-5144.
- (134) Oelbner, W.; Berthold, F.; Guth, U. The IR drop—well-known but often underestimated in electrochemical polarization measurements and corrosion testing. *Mater. Corros.* **2006**, *57*, 455-466.
- (135) Stedwell, C. N.; Polfer, N. C. Spectroscopy and the electromagnetic spectrum. In *Laser photodissociation and spectroscopy of mass-separated biomolecular ions*; Polfer, N. C., Dugourd, P., Eds.; Springer Denmark: Cham, 2013; pp 1-20.
- (136) Bunaciu, A. A.; Udristioiu, E. G.; Aboul, E. H. Y. X-ray diffraction: instrumentation and applications. *Crit. Rev. Anal. Chem.* **2015**, *45*, 289-299.
- (137) Langford, J. I.; Wilson, A. Scherrer after sixty years: a survey and some new results in the determination of crystallite size. *J. Appl. Crystallogr.* **1978**, *11*, 102-113.
- (138) Zhou, W.; Apkarian, R. P.; Wang, Z. L.; Joy, D. Fundamentals of Scanning electron microscopy (SEM). In *Scanning microscopy for nanotechnology: techniques and applications*; Zhou, W., Wang, Z. L., Eds.; Springer New York: NY, 2007; pp 1-39.
- (139) Yathisha, R.; Nayaka, Y. A.; Purushothama, H.; Manjunatha, P.; Basavarajappa, K.; Vinay, M. Investigation the influence of Zn²⁺ doping on the photovoltaic properties (DSSCs) of MgO nanoparticles. *J. Mol. Struct.* **2020**, *1217*, 128407.
- (140) Moscone, D.; D'ottavi, D.; Compagnone, D.; Palleschi, G.; Amine, A. Construction and analytical characterization of prussian blue-based carbon paste electrodes and their assembly as oxidase enzyme sensors. *Anal. Chem.* **2001**, *73*, 2529-2535.
- (141) Svancara, I.; Vytras, K.; Barek, J.; Zima, J. Carbon paste electrodes in modern electroanalysis. *Crit. Rev. Anal. Chem.* **2001**, *31*, 311-345.